



ENSO and internal sea surface temperature variability in the tropical Indian Ocean since the Maunder Minimum

Maike Leupold¹, Miriam Pfeiffer², Takaaki K. Watanabe³, Lars Reuning², Dieter Garbe-Schönberg², Chuan-Chou Shen^{4,5,6}, Geert-Jan A. Brummer⁷

5 ¹EMR-Group, Geological Institute, RWTH Aachen University, Aachen, 52062, Germany

²Institute of Geosciences, Kiel University, Kiel, 24118, Germany

³Department of Natural History Sciences, Faculty of Science, Hokkaido University, Sapporo, 060-0810, Japan

⁴High-Precision Mass Spectrometry and Environment Change Laboratory (HISPEC), Department of Geosciences, National Taiwan University, Taipei, 10617, Taiwan ROC

10 ⁵Research Center for Future Earth, National Taiwan University, Taipei, LC6L73, Taiwan ROC

⁶Global Change Research Center, National Taiwan University, Taipei, 10617, Taiwan, ROC

⁷Department of Ocean Systems, Royal Netherlands Institute for Sea Research (NIOZ), and Utrecht University, 1790 AB Den Burg, The Netherlands

15 *Correspondence to:* Maike Leupold (maike.leupold@emr.rwth-aachen.de)

Abstract. The dominant modes of climate variability on interannual timescales in the tropical Indian Ocean are the El Niño Southern Oscillation (ENSO) and the Indian Ocean Dipole. El Niño events have occurred more frequently during recent decades and it has been suggested that an asymmetric ENSO teleconnection (warming during El Niño events is stronger than cooling during La Niña events) caused the pronounced warming of the western Indian Ocean. In this study, we test this hypothesis using coral Sr/Ca records from the central Indian Ocean (Chagos Archipelago) to reconstruct past sea surface temperatures (SST) in time windows from the Maunder Minimum to the present. Three sub-fossil massive *Porites* corals were dated to the 17-18th century (one sample) and 19-20th century (two samples), and were compared with a published, modern coral Sr/Ca record from the same site. All corals were sub-sampled at a monthly resolution for Sr/Ca measurements, which were measured using a simultaneous ICP-OES. All four coral records show typical ENSO periodicities, suggesting that the ENSO-SST teleconnection in the central Indian Ocean was stationary since the 17th century. To determine the symmetry of ENSO events, we compiled composite records of positive and negative ENSO-driven SST anomaly events. We find similar magnitudes of warm and cold anomalies indicating a symmetric ENSO response in the tropical Indian Ocean. This suggests that ENSO is not the main driver of central Indian Ocean warming.



1 Introduction

30 In times of increasing impacts of global climate change, paleoclimate research seems more important than ever. Especially the Indian Ocean is of major relevance to global ocean warming as the western Indian Ocean has been warming faster than any



other ocean basing during the last century and is the largest contributor to the current rise of global mean sea surface temperatures (Roxy et al., 2014).

As tropical corals can be used to reconstruct past changes of environmental parameters, such as sea surface temperatures (SST),
35 by measuring Sr/Ca , they can help to determine changes in past climate variabilities. Most coral paleoclimatological studies covering periods before 1900 conducted in the tropical Indian Ocean predominantly focused on $\delta^{18}\text{O}$ measurements (e.g. Abram et al., 2015; Charles et al., 2003; Cole et al., 2000; Nakamura, et al., 2011; Pfeiffer et al., 2004). There are only some studies including Sr/Ca measurements for SST reconstructions (e.g. Pfeiffer et al., 2006), while few studies included Sr/Ca measurements for SST reconstructions (e.g. Pfeiffer et al., 2006). Most studies are focusing on either the western or the eastern
40 Indian Ocean (Abram et al., 2003; Watanabe et al., 2019) and/or are sampled at only bimonthly (Zinke et al., 2004; Zinke et al., 2008) or annual resolution (Zinke et al., 2014; Zinke et al., 2015). The lack of data in the central, tropical Indian Ocean still limits the understanding of the relationship between interannual and decadal climate variabilities in the tropical Indian Ocean associated with transregional or global climate phenomena.

Strong El Niño/Southern Oscillation (ENSO) events occur more frequently since the early 1980s (Baker et al., 2008; Sagar et al., 2016) and have a strong influence on the tropical Indian Ocean demonstrating an existing stable SST-ENSO teleconnection between the Pacific Ocean and Indian Ocean (Pfeiffer & Dullo, 2006; Wieners et al., 2017). In fact, it was suggested that El Niño events have a stronger influence on the Indian Ocean than La Niña events (Roxy et al., 2014). In their study, Roxy et al. (2014) propose that El Niño events cause strong warming of the western Indian Ocean, whereas La Niña events do not cause significant cooling of the region. This asymmetric ENSO teleconnection has been suggested to contribute to the overall
50 warming of the tropical Indian Ocean. Here, we test this hypothesis using three sub-fossil massive *Porites* coral samples and one modern coral core from the central Indian Ocean (Chagos Archipelago) to reconstruct past SST. The modern core was included in a composite reconstruction of large-scale SST (Pfeiffer et al., 2017) and the core top (1950-1995) was shown to record SST variability at Chagos on grid-SST scale (Pfeiffer et al., 2009). The sub-fossil corals record 41 years of the Maunder Minimum (1675-1716), 31 years of the late Little Ice Age (1836-1867) and 39 years of the mid-19th to early 20th century
55 (1870-1909) covering 39 years. We identify past warm and cold events in each record and use these events to compile composites to evaluate the symmetry of positive and negative ENSO-driven SST anomaly events in the tropical Indian Ocean.

2 Regional setting

2.1 Location

The Chagos Archipelago is located in the tropical Indian Ocean, about 500 km south of the Maldives. It consists of several
60 atolls with islands, submerged and drowned atolls, and other submerged banks with the Great Chagos Bank being the world's largest atoll (Fig. 1). The Great Chagos Bank covers an area of 18.000 km² with eight islands totaling 445 ha of land. Its lagoon has a maximum depth of 84 m and a mean depth of 50 m. Due to its large size and submerged islands, water exchange with the open ocean is substantial. The Salomon atoll is located about 135 km towards the northeast of Eagle Island. Its atoll area



is about 38 km² and has an enclosed lagoon and an island area > 300 ha. The greatest depth of its lagoon is 33 m, with mean
65 depth of 25 m.

2.2 Climate

Chagos is situated in a region characterized by monsoon climate (Sheppard et al., 2012). The austral summer is the wet season, with the Northeast monsoon lasting from October to February (Pfeiffer et al., 2004). From October to April, light to moderate north-west trades blow. During the rest of the year, strong winds from the southeast dominate (Sheppard et al., 1999).

70 Chagos lies at the eastern rim of the so-called Seychelles-Chagos thermocline ridge (SCTR). Along that region, a shallow thermocline causes open-ocean upwelling of cold waters. Upwelling along this region was first identified by McCreary et al. (1993) and is forced by both negative and positive wind stress curl (Hermes & Reason, 2009; McCreary et al., 1993). Compared to other upwelling regions of the Indian Ocean, the sea surface temperatures of the SCTR are relatively high. They vary between 28.5°C and 30°C in austral summer. The SCTR is believed to play a major role in the climate variability of this region
75 on different timescales (e.g. Hermes & Reason, 2008; Vialard et al., 2009) with very strong air-sea interaction due to open ocean upwelling combined with relatively warm SST (Sheppard et al., 2012).

On interannual timescales, the dominant mode of climate variability in the SCTR is the El Niño Southern Oscillation (ENSO). During El Niño events, the West Pacific warm pool is displaced towards the East resulting in cooler than normal SST in the Western Pacific and a basin-wide warming of the Indian Ocean (Izumo et al., 2014; Sheppard et al., 2013). Figure 2 compares
80 the positive SST anomalies during El Niño with the negative SST anomalies during La Niña events in the Indian and Pacific Ocean between 1982 and 2016, as inferred from ‘Reynolds’ OI v2 SST data (Reynolds et al., 2002; averaged over December-February). Even if not as strong as in the Pacific Ocean, an ENSO response in the tropical Indian Ocean can be observed (Fig. 2). Coupled ocean-atmosphere instabilities centered in the tropical Indian Ocean result in Indian Ocean Dipole (IOD) events (Saji et al., 1999; Sheppard et al., 2013; Webster et al., 1999). A negative (positive) IOD event is defined by warmer (cooler)
85 than normal SST in the eastern part of the Indian Ocean and cooler (warmer) than normal SST in the western Indian Ocean. Several studies showed that the IOD is an inherent mode of variability of the Indian Ocean (e.g. Ashok et al., 2003; Krishnaswamy et al., 2015; Saji et al., 1999; Webster et al., 1999). However, IOD events tend to co-occur with ENSO events (e.g. Luo et al., 2010; Saji and Yamagata, 2003). The instrumental record of past IOD events does not go back further than 1960 (Saji and Yamagata, 2003). A coral-based reconstruction of past IOD events extends until 1846 and suggests a recent
90 intensification of the IOD (Abram et al., 2008). The coral index shows few strong IOD events in the 20th and late 19th century (i.e. 1997/98, 1961 and 1877/78), of which only the event in 1961 is independent of ENSO (Abram et al., 2008).

We therefore decided to treat positive SST anomaly events found in our records as El Niño events even if they could be a result of IOD events independent from or overlapping with ENSO events.



2.3 Instrumental data

95 High-resolution SST data of the AVHRR satellite product (Casey et al., 2010) reveal different mean SST and seasonality at
Chagos depending on the reef setting (Leupold et al., 2019; Fig. 3). At the open ocean reefs, where ocean upwelling occurs,
seasonal minima in SST are more pronounced than in the lagoon, whereas maximum temperatures are not significantly
different (t-value = 0.27; p-value = 0.79). Averaged over the entire area of the Chagos (70-74° E; 4-8° S), SST is similar to
SST measured in the lagoon. Long-term monthly SST anomalies (i.e. mean seasonal cycle removed) reveal that extreme SST
100 events, such as El Niño in 1997/98 or La Niña in 2010/11, have the same magnitude in both lagoon and open ocean settings
(Fig. 3b). Both anomaly records are not significantly different (t-value = 0.34; p-value = 0.37). This suggests that the
magnitudes of ENSO signals at Chagos should be recorded in all coral records analyzed in this study, as it is independent from
the reef setting.

2.4 ENSO indices

105 **The instrumental record of past ENSO events is restricted to the late 19th and early 20th century.** Nino 3.4 SST anomalies are
taken from NOAA ERSSTv5 (Huang et al. 2017). These have been interpolated from sparse observational data and extend
back until 1870. The annual El Niño Index *Nino3.4* (Wilson et al., 2010), which was reconstructed using data from the
central Pacific (corals), the **TexMex** region of the USA (tree rings) and other regions in the Tropics (corals and an ice core),
was used as a time series of past ENSO events that extends beyond the instrumental period, until 1607. Evidence for the
110 occurrence and magnitude of historical ENSO events have been compiled in **Quinn (1993) extending back until 1500.** As this
reconstruction is based on historical observations of various aspects of ENSO, it should be relatively independent from
statistical biases. Additionally, Brönnimann et al. (2006) obtained a balanced view of ENSO events (both El Niño and La Niña
events) by combining several reconstructed ENSO indices, climate field reconstructions and early instrumental data. Their
reconstruction period extends back to 1500 (La Niña events) and 1511 (El Niño events), respectively.

115 3 Methods and materials

3.1 Coral collection and preparation

For this study, three sub-fossil coral samples were collected in February 2010, from boulder beaches and derelict buildings of
former settlements at Chagos (Fig. S1). Samples E3 (1870-1909) and E5 (1675-1716) were taken from Eagle Island (S
6°11.39'; E 71°19.58'), an island on the western rim of the Great Chagos Bank (Fig. 1). Sample B8 (1836-1867) was taken
120 from the lagoon-facing site of Boddam Island (S 5°21.56'; E 72°12.34') in the southwestern part of the Salomon atoll. The
samples were cross-sectioned into 0.7-1.0 cm thick slabs and X-rayed.

Core GIM, a modern core described in previous publications (Pfeiffer et al., 2004; Timm et al., 2005; Pfeiffer et al., 2009;
Pfeiffer et al., 2017) was drilled underwater in 1995 in the lagoon of Peros Banhos, located in the northwest of Chagos. The
monthly coral Sr/Ca record of GIM extends from 1880-1995. Analytical procedures have been described in Pfeiffer et al.



125 (2009). The core top (1950-1995) was shown to record SST variability at Chagos on a grid-SST scale (Pfeiffer et al., 2009).
The entire record was included in a composite reconstruction of large-scale western Indian Ocean SST (Pfeiffer et al., 2017).
In this study, we use this core to estimate the magnitude of modern ENSO events.
From the slabs of the sub-fossil corals, powder samples were drilled at 1 mm increments using a micro-milling machine (type
PROXXON FF 500 CNC). This depth resolution can be translated to monthly temporal resolution with average growth rates
130 being 12 mm/yr. The subsampling paths were always set along the optimal growth axis that was determined based on x-ray
images (Fig. S2).

3.2 Coral Sr/Ca analysis

Sr/Ca ratio measurements were performed at Kiel University using a Spectro Ciros CCD SOP inductively coupled plasma
optical emission spectrometer (ICP-OES). Elemental emission signals were simultaneously collected and subsequently
135 processed following a combination of techniques described by Schrag (1999) and de Villiers et al. (2002). Between 0.13 and
0.65 mg of coral powder was dissolved in 1.00 mL 0.2 M HNO₃. Prior to analysis, the solution was diluted with 0.2 M HNO₃
to a final concentration of approximately 8ppm Calcium. Strontium and Calcium intensity lines used are 421 nm and 317 nm,
respectively. The intensities of Strontium and Calcium were converted into Sr/Ca ratios in mmol/mol. An in-house coral
reference standard (Mayotte) was measured after every six samples and was used for drift-correction of the measured Sr/Ca
140 ratios. Average analytical precision of Sr/Ca measurements as estimated from sample replicates was typically around 0.08 %
RSD, translating into a temperature of less than 0.2°C.

3.3 Chronology

Each sub-fossil coral sample was dated by U-Th in 2016. U-Th isotopic measurements were performed with an MC-ICPMS
(Thermo Electron Neptune) in the High-Precision Mass Spectrometry and Environment Change Laboratory (HISPEC) of the
145 Department of Geosciences, National Taiwan University (NTU), following techniques described in Shen et al. (2012). U-Th
isotopic compositions and concentrations are listed in Table 1.

The chronology of the samples was developed based on seasonal cycles of coral Sr/Ca and by analyzing the density bands
visible on x-ray images (Fig. S2). We assigned the highest Sr/Ca value to the SST minimum of each year and interpolated
linearly between these anchor points to obtain a time series with equidistant time steps.
150 Sample E5 covers the period from 1675 to 1716, herein further referred to as E5 (1675-1716). Sample B8 covers the period
from 1836 to 1867, E3 from 1870 to 1909, both referred to as B8 (1836-1867) and E3 (1870-1909), respectively. The
uncertainties of the age models are approximately ±1.9 years (E5), ±2.2 years (B8) and ±2.4 years (E3). All age models were
verified by a second, independently measured U-Th age of each sample, measured in 2017 in the HISPEC laboratory of the
Department of Geosciences, NTU, following techniques described in Shen et al. (2012). These age determinations are
155 consistent with our Sr/Ca chronologies.



3.4 Diagenesis screening

A combination of X-ray diffraction (XRD), optical and scanning electron microscopy (SEM) was used to investigate potential diagenetic alteration in the sub-fossil coral samples from Chagos that may affect the Sr/Ca values (Figs. S3, S4, and S5).

160 Representative samples for thin-section, scanning electron microscopy (SEM) and X-ray diffraction (XRD) analysis were selected from all corals based on the X-ray images. The 2-D-XRD system Bruker D8 ADVANCE GADDS at the Rheinisch-Westfaelische Technische Hochschule (RWTH) Aachen was used for non-destructive XRD point-measurements directly on thin-section blocks with a calcite detection limit of $\sim 0.2\%$ (Smodej et al., 2015). For each coral sample diagenetic modifications were analyzed using one thin-section, one sample for SEM, one 2D-XRD measurement and one powder-XRD measurement.

165 3.5 Statistics

Composite were generated calculating the mean of positive and negative anomaly events taken from centered monthly coral SST anomaly records. By centering the coral records to their mean and focusing on interannual variability, we eliminate the largest uncertainty of single-core Sr/Ca records, as it known from Sayani et al. (2019) that generating a composite Sr/Ca record using five coral sample records instead of one coral record offers a ca. 2.5 times smaller error in mean SST reconstructions.

170 Power spectra analysis was performed twice using the open source software *PAST* (Hammer et al., 2001). One run was performed with the time series before detrending them, one run after detrending. All time series were detrended using the softwares *breakfit* (Mudelsee, 2009) or *rampfit* (Mudelsee, 2000), respectively (Fig. S6).

Singular spectrum analysis (SSA) (Vautard & Ghil, 1989) and **wavelet coherence plots** were generated using the *MATLAB* software toolboxes.

175 T-test were conducted using the free web application *T-Test Calculator* (GraphPad QuickCalcs, 2019).

As the significance of the means calculated for the composite records depends on the numbers of events, standard errors (SE) were used and calculated as follows:

$$SE = \frac{\text{standard deviation } (\sigma)}{\sqrt{\text{Number of events } (n)}}, \quad (1)$$

4 Results and Interpretation

180 4.1 Diagenesis

Only trace amounts of diagenetic phases were detected in the sub-fossil coral samples, which show a good to excellent preservation according to the criteria defined in Cobb et al. (2013). Isolated scalenohedral calcite cement crystals were observed in the thin-section of E5 (1675-1716) (Fig. S3 a-d). However, XRD results and SEM analysis confirm that the calcite abundance is below the detection limit of XRD (0.2%) in this sample (Fig. S3 e-f). B8 (1836-1867) shows trace amounts of **patchily** distributed, thin aragonite cements (Fig. S4 a-f). E3 (1870-1909) is devoid of diagenetic phases (Fig. S4 a-f), but in

185



some areas of the thin-section dissolution of centers of calcification can be seen (Fig. S5 c-d). Slight dissolution and microborings are also visible under SEM (Fig. S5 f). However, microborings are always open and therefore will not influence the geochemistry.

4.2 Sr/Ca measurements

190 Table 2 gives an overview of the Sr/Ca ratios of each sub-fossil coral core and statistical key figures of the records. All coral Sr/Ca records were centered, i.e. normalized with respect to their mean values (Pfeiffer et al., 2009) and translated into SST using a temperature dependence of -0.06 mmol/mol per 1°C for Porites corals at Chagos (Leupold et al., 2019; Pfeiffer et al., 2009). The values are shown in Figure 4.

4.2.1 17-18th century

195 A total of 472 subsamples from E5 (1675-1716) was measured for Sr/Ca. The average Sr/Ca value is 8.96 ± 0.07 mmol/mol. The range of all Sr/Ca values over the 41-year sample span is 0.41 mmol/mol, between a minimum of 8.73 mmol/mol and a maximum of 9.14 mmol/mol.

4.2.2 19-20th century

200 From B8 (1836-1867), Sr/Ca of 375 subsamples was measured. The average value is 9.02 ± 0.07 mmol/mol over a range of 0.506 mmol/mol. The maximum Sr/Ca value for the 31-year sample span is 9.36 mmol/mol, the minimum Sr/Ca value is 8.85 mmol/mol.

For E3 (1870-1909), Sr/Ca measurements were conducted on 415 subsamples. The average Sr/Ca value is 8.95 ± 0.06 mmol/mol for the 39-year sample span, over a range of 0.376 mmol/mol from a minimum value of 8.79 mmol/mol to a maximum of 9.17 mmol/mol.

205 4.3 Seasonal cycle

The mean annual cycles of all sub-fossil coral SST records are not significantly different as indicated by p-values around 1 in the t-tests (Table 3). The seasonal amplitudes in coral SST [$^{\circ}\text{C}$] are slightly higher in E5 (1675-1716) (1.99°C) compared to B8 (1836-1867) (1.81°C) and E3 (1870-1909) (1.71°C). A shift of mean maximum temperatures from February (E5 and B8) to April (E3) can be observed (Fig. 4). Seasonal amplitudes explain 26-32% of the coral-SST variance (see supplementary material and Fig. S7).

210

4.4 ENSO Interannual SST variability

The modern and the sub-fossil coral SST records were compared with the annually resolved El Niño index $Niño3.4$ that extends back until 1607 (Wilson et al., 2010) and the monthly resolved $Niño3.4$ index based on NOAA ERSSTv5 (Huang et al., 2017;





only used for power spectrum analysis). All coral records show positive and negative SST anomalies, which occur in years
215 where ENSO (positive and negative) events have been reported (Fig. 5). For a better comparison of the coral SST records' and
the *Niño*3.4 index' frequencies, power spectra of detrended time series were computed (Fig. 6). All coral SST records show
the typical ENSO periodicity between 3 and 8 years (Fig. 6a-d). Those periodicities can also be found in the power spectra of
the *Niño*3.4 indexes (Fig. 6e & f). Even after detrending, the power spectrum of the GIM coral SST record still shows the
highest power at low-frequencies, which translates to a period of 21-22 years. This cannot be explained by ENSO activities,
220 but may be related to tropical Pacific forcing (Pfeiffer et al., 2009). The power spectrum analysis results were confirmed by
both singular spectrum analysis (SSA; Figs. S8-S10) and Wavelet coherence analysis (Fig. S11) results (see supplementary
material).

All coral records show variations in the frequency of ENSO events (Figs. 7-9 and Tables 4-6). Our results show that, compared
to the 17-18th century, ENSO events are more frequently recorded in coral records of the central Indian Ocean in recent
225 periods: According to the AVHRR satellite data and coral records, an El Niño event occurs on average every 4 years between
1981 and 2017 (AVHRR) or every 5 years between 1965 and 1995 (coral record), respectively (see Figs. 7 & 9 and Tables 4-
6). This is supported by the events listed in Quinn (1993). The average recurrence interval for the period that covers the coral
E5 (1675-1716) record is 5.1 yrs, whereas it is 3.6 yrs between 1965 and 1995. The same holds for the negative SST anomaly
events (La Niña and non-La Niña events): based on the AVHRR satellite data and the coral records, negative anomaly events
230 occurred more frequently between 1981 and 2017 (every 2.6 years; AVHRR) and between 1965 and 1995 (every 6 years in
the coral record or 5 yrs in Brönnimann et al., 2006), respectively, than during the 17-18th century. For the 17-18th century,
the recurrence interval for negative SST anomalies is only 6.8 years (coral record) or 10.3 yrs (Brönnimann et al., 2006) (see
Figs. 8 & 9 and Tables 4 & 5).

4.5 ENSO composites

235 Composites of monthly coral SST anomalies were produced for ENSO (positive and negative) events to assess their
magnitudes. Each composite was produced using coral records of several individual ENSO events. An overview of the events
used for generating each composite can be found in Table 4 and Table 5. An overview of all events found in the coral Sr/Ca
records and of ENSO events of the corresponding time periods listed in Quinn (1993) and Brönnimann et al. (2006) is given
in Table 6. Positive SST anomalies in the coral records were interpreted as positive ENSO events when the year of occurrence
240 was listed as one with large-scale ENSO event in Quinn (1993) and Brönnimann et al. (2006) within the error of each coral
age model and when the anomaly exceeds 1.5 standard deviations of the mean of each coral record (Fig. S6). In addition to the
strong La Niña events listed in Brönnimann et al. (2006), we added negative SST anomalies occurring in years after the El
Niño years to the composite.

The composite record for El Niño events comprises 35 events, and 31 events for the La Niña composite (Table 4). To
245 investigate changes in the magnitude of ENSO anomalies over time, composites for the time periods 17-18th century and 19-
20th century, respectively, were generated. For the 17-18th century, six events (five events) were used for the El Niño (La



Niña) composite. For the composite for the 19-20th century, we included events taken from the GIM record. For the 19-20th century, 29 events (26 events) were used for the El Niño (La Niña) composite. The 19-20th century composites, in turn, were split into three sub-periods: 1830-1929 (18 El Niño events, 16 La Niña events), 1930-1964 (five El Niño events, five La Niña events; Table 5) and 1965-1995 (six El Niño events, five La Niña events). These sub-periods were chosen because ENSO activity was reduced between 1930 and 1965 compared to before 1930 and after 1965 (e.g. Cole et al., 1993).

Observations indicate that some upwelling events in the central Indian Ocean are not forced by large-scale ENSO or IOD variability but associated with cyclonic wind stress curls in the southern tropical Indian Ocean (Dilmahamod et al., 2016; Hermes & Reason, 2009). Such an upwelling event occurred in August 2002 and was found in both the coral and satellite SST records at Chagos (see Leupold et al., 2019). To investigate the effect of these negative anomaly events on the La Niña composites, the 19-20th century composites were split up into composites of La Niña events and other negative anomaly events, which are not related to La Niña. La Niña and negative anomalies other than La Niña events were selected based on the months they occurred in, i.e. November-May (La Niña), June-September (Non-La Niña).

As such events are also observed recently, we compared modern (1981-2018) satellite SST composites for El Niño events (nine events), La Niña events (10 events) and negative anomalies other than La Niña events (four events) with our coral SST composites. We used the AVHRR satellite SST (Casey et al., 2010) averaged over entire Chagos (4-8° S; 70-74° W). All SST anomalies were generated by subtracting the long-term monthly mean from each monthly mean SST value and converting coral Sr/Ca into SST using a temperature dependence of -0.06 mmol/mol per 1°C (see Leupold et al., 2019).

4.5.1 Positive anomalies in coral and satellite SST composites

Coral SST proxy of the central Indian Ocean record similar, but higher anomalies during El Niño events compared to the satellite composites (Fig. 7), which may reflect the greater sensitivity of the corals to reef-scale temperatures (Leupold et al., 2019) or the different time periods covered by these records (only two El Niño events in the AVHRR record overlap with the coral data). The coral composite records of the 17-18th century show higher anomalies than the coral composites of the 19-20th century (Fig. 7).

All positive SST anomalies identified as El Niño events in the coral records show on average a maximum value of $1.5 \pm 0.1^\circ\text{C}$ (Fig. 7). The average maximum temperature anomaly value of El Niño events during the 17-18th century were $2.2 \pm 0.2^\circ\text{C}$, higher than and significantly different ($p \ll 0.01$) from the average maximum El Niño temperature anomaly during the 19-20th century ($1.3 \pm 0.1^\circ\text{C}$). The average maximum temperature of El Niño events picked from the AVHRR satellite SST (covering the period from 1981 to 2018) of $0.8 \pm 0.1^\circ\text{C}$ is also lower than and significantly different ($p \ll 0.01$) from those in the 19-20th century. This suggests a greater impact of El Niño events on Indian Ocean SST during the 17-18th century compared to the 19-20th century and during the last decades.



4.5.2 Negative anomalies in coral and satellite SST composites

No statistically significant differences were found between negative anomalies in coral SST in the central Indian Ocean during the 17-18th century and the 19-20th century and between La Niña and non-La Niña events (Fig. 8).

280 All negative SST anomalies identified as La Niña and non-La Niña events in the coral records show a minimum temperature anomaly of $-1.6 \pm 0.1^\circ\text{C}$ on average (Fig. 8). The average minimum temperature anomalies of La Niña and non-La Niña events during the 17-18th century were slightly less extreme ($-1.5 \pm 0.3^\circ\text{C}$), but not significantly different ($p = 0.73$) from the average minimum temperature anomalies of the 19-20th century ($-1.6 \pm 0.2^\circ\text{C}$).

285 Separating the composites into La Niña and non-La Niña events shows that La Niña events in the coral records are slightly more negative, but not statistically different from non-La Niña events ($p = 0.60$). The same is observed in the AVHRR satellite SST anomaly composites, where average La Niña minimum temperature anomalies are $-0.8 \pm 0.1^\circ\text{C}$ and non-La Niña anomalies are $-0.6 \pm 0.1^\circ\text{C}$ ($p = 0.17$).

On average, the minimum temperature anomaly is $-1.6 \pm 0.1^\circ\text{C}$ for all La Niña events and $-1.5 \pm 0.4^\circ\text{C}$ for La Niña events during the 19-20th century of the coral SST records ($p = 0.75$).

290 4.5.3 Interannual SST anomalies during the 19th and 20th century

Dividing the 19-20th century into three sub-periods (1830-1929; 1930-1964; 1965-1995) and compiling SST anomaly composites allows us to assess changes the magnitude of ENSO-driven warm and cold anomalies over time (Fig. 9). The El Niño composites do not show any systematic changes during the 19-20th century in the Indian Ocean For the period between 1830 and 1929, the average maximum temperature anomaly is $1.4 \pm 0.1^\circ\text{C}$, while between 1930 and 1964 the average maximum temperature anomaly of $1.2 \pm 0.1^\circ\text{C}$ is slightly less extreme than the previous period, but not significantly different ($p = 0.5$). For the last period of the 20th century, 1965 to 1995, the average maximum temperature anomaly is again to $1.4 \pm 0.1^\circ\text{C}$ (Fig. 9). The magnitude of cooling during La Niña and non-La Niña events tend to reduce from 1830-1929 to 1965-1995 (Fig. 9).

300 For the period between 1830 and 1929, the average minimum temperature anomaly is $-1.9 \pm 0.2^\circ\text{C}$. Between 1930 and 1964 the average minimum temperature anomaly increases by 0.58°C to $-1.3 \pm 0.1^\circ\text{C}$, and for 1965 to 1995, the average minimum temperature anomaly is $-1.1 \pm 0.1^\circ\text{C}$. However, for both El Niño and La Niña events, the differences between the means of the first period (1830-1929) and the last period (1965-1995) are not statistically significant ($p = 0.93$; $p = 0.07$, respectively).

5 Discussion

305 During the 17-18th and 19-20th century, all coral records show typical ENSO periodicities in their SSA, power spectra and/or wavelet analysis. We therefore can say that the ENSO teleconnection to SST in the central Indian Ocean was stable back until the Maunder Minimum, consistent with previous studies that showed a stable ENSO-SST teleconnection over the late 19th



and early 20th century (Pfeiffer and Dullo, 2006). Overall, predominantly strong ENSO events are recorded by the coral records from Chagos, as indicated in the list of events presented in (Brönnimann et al, 2006) (Table 6).

The coral record dated to the 17-18th century covers a period of long-term cooling and succeeds periods of initially reduced ENSO activity between the early 1500s and early 1600s (Hereid et al., 2013), followed by a phase of protracted ENSO events in the 1620s (Grove, 2018). Between the early 15th to middle 17th century, average amplitudes of El Niño events appear to be similar to modern coral records in the West Pacific (Hereid et al., 2013). Furthermore, it is described that ENSO events in the first half of the 17th century resulted in the failure of the India monsoon and thus, in droughts and famines in South India (Grove, 2018). Our 17-18th century coral record with its higher amplitudes of El Niño events but generally fewer ENSO events (relative to modern satellite and coral records) reflects both the observations summarized in Grove (2018) and the reduced ENSO activity as found in Hereid et al. (2013). This suggests a shift towards an increased ENSO activity around the first half of the 17th century back to a reduced ENSO activity, but with higher amplitude (El Niño) events compared to modern ones. Furthermore, our results show that El Niño events resulted in stronger SST anomalies in central Indian Ocean corals in the 17-18th century, i.e. during a cooler mean climate, than they did in the 19th and 20th century. This result is consistent with Pfeiffer et al., (2017), who found larger amplitude El Niño events in the late 19th century, when mean SSTs in the tropical Indian Ocean were cooler. It is also consistent with Zinke et al. (2004) who found highest $\delta^{18}\text{O}$ amplitude variations in the interannual ENSO band between 1645–1715 in a coral from Ifaty, Madagascar. Comparing both periods, the La Niña and non-La Niña events show no significant changes suggesting a stable negative SST anomaly pattern in the Indian Ocean.

Overall, the magnitudes of El Niño and La Niña events recorded in the Chagos coral records during the past century are comparable (Fig. 9). This suggests the ENSO teleconnection in the tropical Indian Ocean remained symmetric. Only in times of cooler mean climates, the corals seem to indicate higher amplitude ENSO-induced warm anomalies in the tropical Indian Ocean, although these differences are not statistically significant. Hence, our results do not support the notion that an asymmetric ENSO teleconnection with strong warming during El Niño years drives the recent warming of the tropical Indian Ocean as suggested by Roxy et al. (2014). The modern coral records from the western Indian Ocean all show a steady warming during the 20th century, and this warming continuous in the time interval of reduced ENSO activity between 1930 and 1965 (e.g. Charles et al., 1997; Pfeiffer and Dullo, 2006; Abram et al., 2016). This suggests that neither the magnitude, nor the frequency of past ENSO events explains the centennial-scale warming of the Indian Ocean.

The coral records from Chagos also record upwelling events in boreal summer, which are independent of ENSO, poorly represented in satellite data of SST (see Leupold et al., 2019), and which may result in the failure of the Indian monsoon. Such an upwelling event occurred for example in 2002 and lead to a drought over the Indian subcontinent (Jayakumar & Gnanaseelan, 2012; Krishnan et al., 2006). At present, little is known about the frequency or magnitudes of these events in past decades or centuries. Coral proxy data from Chagos thus allow us to better understand these events non-La Niña upwelling events.

In contrast to the stable teleconnection between ENSO and SST in the central Indian Ocean, the ENSO-precipitation teleconnection was shown to be non-stationary (Timm et al., 2005). The impact of ENSO on rainfall in the central Indian



Ocean depends on mean SSTs, and these surpassed a critical threshold for atmospheric convection in the mid-1970s, strengthening the El Niño signal in rainfall. However, our study does not indicate an increase in the magnitude of El Niño-related SST anomalies following this shift compared to earlier time periods of strong ENSO activity.

In summary, this study confirms that the ENSO-SST teleconnection between the Pacific and Indian Ocean is stationary over
345 the 19th/20th century and back into the Maunder Minimum. We have shown that it is possible to reconstruct interannual SST
variations in the tropical Indian Ocean. This is important because so far there exist no reliable high-resolution SST
reconstructions in the Indian Ocean covering the periods we studied. SST reconstruction studies of the Pacific Ocean also
show ENSO and decadal-scale variability covering the periods from 1998 back to 1886 (Cobb et al., 2001) and 928-961, 1149-
1220, 1317-1464 and 1635-1703 (Cobb et al., 2003). Cobb et al. (2003) spliced three overlapping coral records of the 14-15th
350 century and five coral records of the 17-18th century together. We have shown that this approach would be applicable in the
tropical Indian Ocean using sub-fossil corals from boulder beaches and historical buildings. This is important because recent
studies have shown that the tropical Indian Ocean plays a pivotal role in 20th century global temperature rise (Funk et al., 2008;
Roxy et al., 2014; Pfeiffer et al., 2017).

6 Conclusions

We have shown that the ENSO-SST relationship in the central Indian Ocean was stationary since the 17th century. All four
355 coral records showed typical ENSO periodicities, but variations in the frequency of ENSO events and in intensity. Whereas
both El Niño and La Niña events occur more often in modern periods (inferred from satellite and coral records) than in the 17-
18th century, El Niño events were more extreme in the 17-18th century relative to ENSO signals in modern coral (1965-1995)
and satellite (1981-2018) records. El Niño events cause average positive anomalies of $2.2 \pm 0.2^\circ\text{C}$ during the 17-18th century
360 and $1.3 \pm 0.1^\circ\text{C}$ during the 19-20th century, while La Niña events cause average negative anomalies of $-1.5 \pm 0.3^\circ\text{C}$ during the
17-18th century and $-1.6 \pm 0.2^\circ\text{C}$ during the 19-20th century in the central Indian Ocean. However, not all cooling events are
related to La Niña events, but also to processes internal to the Indian Ocean causing negative anomalies of $-1.5 \pm 0.4^\circ\text{C}$ during
the 19-20th century. The magnitudes of El Niño and La Niña events during the last century are comparable indicating a
symmetric ENSO teleconnection. An asymmetric ENSO teleconnection being the cause for the overall warming of the central,
365 tropical Indian Ocean appears therefore unlikely. However, we suggest compiling composite records of negative and positive
SST anomaly events from sub-fossil corals to further test the hypothesis of an asymmetric ENSO teleconnection in the western
Indian Ocean.

Author contribution: M.L. conceived the study, wrote the paper and produced all figures. M.P., L.R., T.K.W. and D.G.-S.
370 helped with analyzing and interpreting the data. L.R. assessed the preservation of the coral samples. T.K.W., C.-C.S. and G.-
J.B. helped dating the samples and with the development of the age models. M.P. acquired the funding for this project,
contributed feedback and helped refine the writing.

Competing interests: The authors declare that they have no competing interests.



Data and materials availability: All methods needed to evaluate the conclusions in the paper are present in the paper and/or the supplementary material. The data plotted in all figures will be available to the public over the Paleoclimatology Branch of NOAA's National Center for Environmental Information (NCEI) (<http://www.ncdc.noaa.gov/data-access/paleoclimatology-data>) after the completion of the dissertation of M. Leupold.

Acknowledgments: We thank Karen Bremer for laboratory assistance and the Deutsche Forschungsgemeinschaft (DFG) for funding the projects PF 676/2-1 and PF 676/3-1. Coral U-Th dating was supported by grants from the Science Vanguard Research Program of the Ministry of Science and Technology, Taiwan, ROC (108-2119-M-002-012), the Higher Education Sprout Project of the Ministry of Education, Taiwan, ROC (108L901001), and National Taiwan University (109L8926).

References

- Abram, N. J., Gagan, M. K., McCulloch, M. T., Chappell, J., and Hantoro, W. S.: Coral reef death during the 1997 Indian Ocean Dipole linked to Indonesian wildfires, *Science*, 301(5635), 952-955, <https://doi.org/10.1126/science.1083841>, 2003.
- Abram, N. J., Gagan, M. K., Cole, J. E., Hantoro, W. S., and Mudelsee, M.: Recent intensification of tropical climate variability in the Indian Ocean, *Nat. Geosci.*, 1(12), 849, <https://doi.org/10.1038/ngeo357>, 2008.
- Abram, N. J., Dixon, B. C., Rosevear, M. G., Plunkett, B., Gagan, M. K., Hantoro, W. S., and Phipps, S. J.: Optimized coral reconstructions of the Indian Ocean Dipole: An assessment of location and length considerations, *Paleoceanogr. Paleocl.*, 30(10), 1391-1405, <https://doi.org/10.1002/2015pa002810>, 2015.
- Abram, N. J., McGregor, H. V., Tierney, J. E., Evans, M. N., McKay, N. P., Kaufman, D. S., ... and Steig, E. J.: Early onset of industrial-era warming across the oceans and continents, *Nature*, 536(7617), 411, <https://doi.org/10.1038/nature19082>, 2016.
- Ashok, K., Guan, Z., and Yamagata, T.: A look at the relationship between the ENSO and the Indian Ocean dipole, *J. Meteorol. Soc. Jpn. Ser. II*, 81(1), 41-56, <https://doi.org/10.2151/jmsj.81.41>, 2003.
- Baker, A. C., Glynn, P. W., and Riegl, B.: Climate change and coral reef bleaching: An ecological assessment of long-term impacts, recovery trends and future outlook, *Estuar. Coast. Shelf. S.*, 80(4), 435-471, <https://doi.org/10.1016/j.ecss.2008.09.003>, 2008.
- Brönnimann, S., Xoplaki, E., Casty, C., Pauling, A., and Luterbacher, J.: ENSO influence on Europe during the last centuries, *Clim. Dynam.*, 28(2-3), 181-197, <https://doi.org/10.1007/s00382-006-0175-z>, 2006.
- Casey, K. S., Brandon, T. B., Cornillon, P. and Evans, R.: The Past, Present and Future of the AVHRR Pathfinder SST Program, in: *Oceanography from Space*, edited by: Barale, V., Gower, J. F. R., and Alberotanza, L., Springer, Dordrecht, NL, 273-287, https://doi.org/10.1007/978-90-481-8681-5_16, 2010.



- 405 Charles, C. D., Hunter, D. E., and Fairbanks, R. G.: Interaction between the ENSO and the Asian monsoon in a coral record of tropical climate, *Science*, 277(5328), 925-928, <https://doi.org/10.1126/science.277.5328.925>, 1997.
- Charles, C. D., Cobb, K. M., Moore, M. D., and Fairbanks, R. G.: Monsoon-tropical ocean interaction in a network of coral records spanning the 20th century, *Mar. Geol.*, 201. [https://doi.org/10.1016/S0025-3227\(03\)00217-2](https://doi.org/10.1016/S0025-3227(03)00217-2), 2003.
- Cheng, H., Edwards, R. L., Shen, C. C., Polyak, V. J., Asmerom, Y., Woodhead, J., ... and Wang, X.: Improvements in ²³⁰Th
410 dating, ²³⁰Th and ²³⁴U half-life values, and U–Th isotopic measurements by multi-collector inductively coupled plasma mass spectrometry, *Earth Planet. Sc. Lett.*, 371, 82-91, <https://doi.org/10.1016/j.epsl.2013.04.006>, 2013.
- Cobb, K. M., Charles, C. D., and Hunter, D. E.: A central tropical Pacific coral demonstrates Pacific, Indian, and Atlantic decadal climate connections, *Geophys. Res. Lett.*, 28(11), 2209-2212, <https://doi.org/10.1029/2001gl012919>, 2001.
- Cobb, K. M., Charles, C. D., Cheng, H., and Edwards, R. L.: El Niño/Southern Oscillation and tropical Pacific climate during
415 the last millennium, *Nature*, 424(6946), 271, <https://doi.org/10.1038/nature01779>, 2003.
- Cobb, K. M., Westphal, N., Sayani, H. R., Watson, J. T., Di Lorenzo, E., Cheng, H., ... & Charles, C. D.: Highly variable El Niño–Southern Oscillation throughout the Holocene, *Science*, 339(6115), 67-70, <https://doi.org/10.1126/science.1228246>, 2013.
- Cole, J. E., Fairbanks, R. G., and Shen, G. T.: Recent variability in the Southern Oscillation: Isotopic results from a Tarawa
420 Atoll coral, *Science*, 260(5115), 1790-1793, <https://doi.org/10.1126/science.260.5115.1790>, 1993.
- Cole, J. E., Dunbar, R. B., McClanahan, T. R., and Muthiga, N. A.: Tropical Pacific forcing of decadal SST variability in the western Indian Ocean over the past two centuries, *Science*, 287(5453), 617-619, <https://doi.org/10.1126/science.287.5453.617>, 2000.
- de Villiers, S., Greaves, M. and Elderfield, H.: An intensity ratio calibration method for the accurate determination of Mg/Ca
425 and Sr/Ca of marine carbonates by ICP-AES, *Geochem. Geophys. Geosy.*, 3(1), 1001, <https://doi.org/10.1029/2001gc000169>, 2002.
- Dilmahamad, A. F., Hermes, J. C., and Reason, C. J. C.: Chlorophyll-a variability in the Seychelles–Chagos Thermocline Ridge: Analysis of a coupled biophysical model, *J. Marine Syst.*, 154, 220-232, <https://doi.org/10.1016/j.jmarsys.2015.10.011>, 2016.
- 430 Funk, C., Dettinger, M. D., Michaelsen, J. C., Verdin, J. P., Brown, M. E., Barlow, M., and Hoell, A.: Warming of the Indian Ocean threatens eastern and southern African food security but could be mitigated by agricultural development, *P. Natl. Acad. Sci USA*, 105(32), 11081-11086, <https://doi.org/10.1073/pnas.0708196105>, 2008.
- GraphPad QuickCalcs: T-Test Calculator, Retrieved from <https://www.graphpad.com/quickcalcs/ttest1/>, last access: 09 April, 2019.
- 435 Grove, R.: El Niño Chronology and the Little Ice Age, in: *The El Niño in world history*, edited by: Grove, R., and Adamson, G., Palgrave Macmillan, London, United Kingdom, 49-79, https://doi.org/10.1057/978-1-137-45740-0_3, 2018.
- Hammer, Ø., Harper, D. A. T., and Ryan, P. D.: Paleontological statistics software: package for education and data analysis, *Palaeontol. Electron.*, (4), 2001.



- Hereid, K. A., Quinn, T. M., Taylor, F. W., Shen, C. C., Edwards, R. L., and Cheng, H.: Coral record of reduced El Niño activity in the early 15th to middle 17th centuries, *Geology*, 41(1), 51-54, <https://doi.org/10.1130/g33510.1>, 2013.
- Hermes, J. C., and Reason, C. J. C.: Annual cycle of the South Indian Ocean (Seychelles-Chagos) thermocline ridge in a regional ocean model, *J. Geophys. Res.-Oceans*, 113(C4), <https://doi.org/10.1029/2007jc004363>, 2008.
- Hermes, J. C., and Reason, C. J. C.: The sensitivity of the Seychelles–Chagos thermocline ridge to large-scale wind anomalies, *ICES J. Mar. Sci.*, 66(7), 1455-1466, 2009.
- Hiess, J., Condon, D. J., McLean, N., and Noble, S. R.: 238U/235U systematics in terrestrial uranium-bearing minerals, *Science*, 335(6076), 1610-1614, <https://doi.org/10.1093/icesjms/fsp074>, 2012.
- Huang, B., Thorne, P. W., Banzon, V. F., Boyer, T., Chepurin, G., Lawrimore, J. H., ... and Zhang, H. M.: Extended reconstructed sea surface temperature, version 5 (ERSSTv5): upgrades, validations, and intercomparisons, *J. Climate*, 30(20), 8179-8205, <https://doi.org/10.1175/jcli-d-16-0836.1>, 2017.
- Ihara, C., Kushnir, Y., Cane, M. A., and Kaplan, A.: Timing of El Niño–related warming and Indian summer monsoon rainfall, *J. Climate*, 21(11), 2711-2719, <https://doi.org/10.1175/2007jcli1979.1>, 2008.
- Izumo, T., Lengaigne, M., Vialard, J., Luo, J. J., Yamagata, T., and Madec, G.: Influence of Indian Ocean Dipole and Pacific recharge on following year’s El Niño: interdecadal robustness, *Clim. Dynam.*, 42(1-2), 291-310, <https://doi.org/10.1007/s00382-012-1628-1>, 2014.
- Jaffey, A. H., Flynn, K. F., Glendenin, L. E., Bentley, W. T., and Essling, A. M.: Precision measurement of half-lives and specific activities of U 235 and U 238, *Phys. Rev. C*, 4(5), 1889, <https://doi.org/10.1103/physrevc.4.1889>, 1971.
- Jayakumar, A., and Gnanaseelan, C.: Anomalous intraseasonal events in the thermocline ridge region of Southern Tropical Indian Ocean and their regional impacts, *J. Geophys. Res.-Oceans*, 117(C3), <https://doi.org/10.1029/2011jc007357>, 2012.
- Krishnan, R., Ramesh, K. V., Samala, B. K., Meyers, G., Slingo, J. M., and Fennessy, M. J.: Indian Ocean-monsoon coupled interactions and impending monsoon droughts, *Geophys. Res. Lett.*, 33(8), <https://doi.org/10.1029/2006gl025811>, 2006.
- Krishnaswamy, J., Vaidyanathan, S., Rajagopalan, B., Bonell, M., Sankaran, M., Bhalla, R. S., and Badiger, S.: Non-stationary and non-linear influence of ENSO and Indian Ocean Dipole on the variability of Indian monsoon rainfall and extreme rain events, *Clim. Dynam.*, 45(1-2), 175-184, <https://doi.org/10.1007/s00382-014-2288-0>, 2015.
- Kumar, K. K., Rajagopalan, B., and Cane, M. A.: On the weakening relationship between the Indian monsoon and ENSO, *Science*, 284(5423), 2156-2159, <https://doi.org/10.1126/science.284.5423.2156>, 1999.
- Kumar, K. K., Rajagopalan, B., Hoerling, M., Bates, G., and Cane, M.: Unraveling the mystery of Indian monsoon failure during El Niño, *Science*, 314(5796), 115-119, <https://doi.org/10.1126/science.1131152>, 2006.
- Leupold, M., Pfeiffer, M., Garbe-Schönberg, D., and Sheppard, C.: Reef-scale-dependent response of massive *Porites* corals from the central Indian Ocean to prolonged thermal stress—evidence from coral Sr/Ca measurements, *Geochem. Geophys. Geosy.*, 20(3), <https://doi.org/10.1029/2018GC007796>, 2019.
- Luo, J. J., Zhang, R., Behera, S. K., Masumoto, Y., Jin, F. F., Lukas, R., and Yamagata, T.: Interaction between El Niño and extreme Indian ocean dipole, *J. Climate*, 23(3), 726-742, <https://doi.org/10.1175/2009jcli3104.1>, 2010.



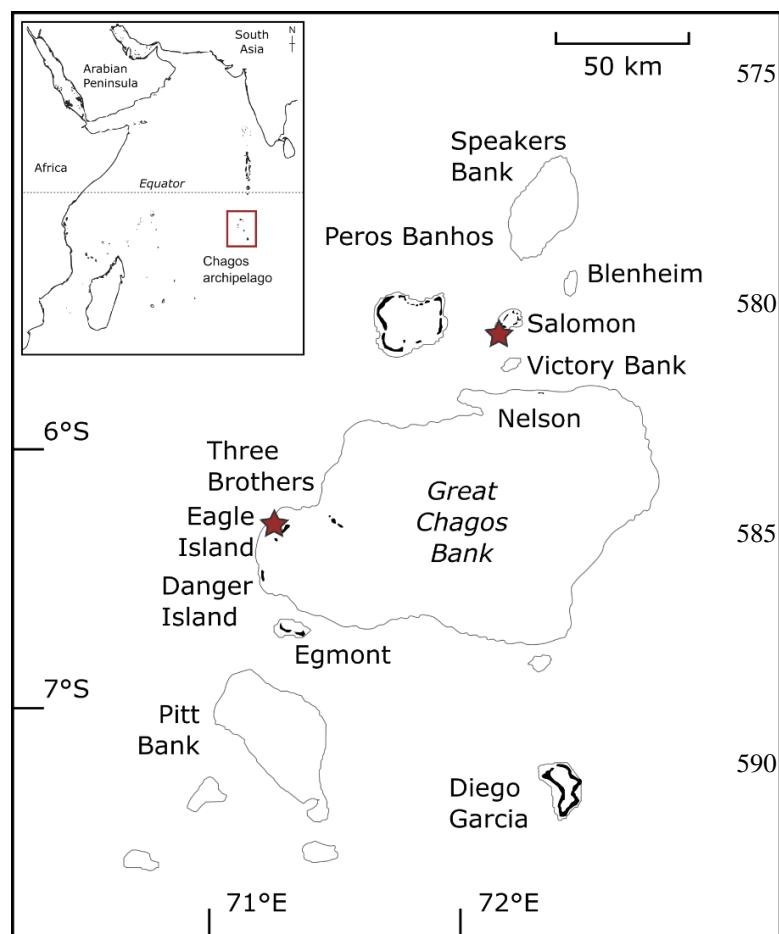
- McCreary, J. P., Kundu, P. K., and Molinari, R. L.: A numerical investigation of dynamics, thermodynamics and mixed-layer processes in the Indian Ocean, *Prog. Oceanogr.*, 31, 181–244, [https://doi.org/10.1016/0079-6611\(93\)90002-u](https://doi.org/10.1016/0079-6611(93)90002-u), 1993.
- 475 Miura, H., Satoh, M., Nasuno, T., Noda, A. T., and Oouchi, K.: A Madden-Julian oscillation event realistically simulated by a global cloud-resolving model, *Science*, 318(5857), 1763-1765, <https://doi.org/10.1126/science.1148443>, 2007.
- Mudelsee, M.: Ramp function regression: A tool for quantifying climate transitions, *Comput. Geosci.-UK*, 26(3), 293-307, [https://doi.org/10.1016/s0098-3004\(99\)00141-7](https://doi.org/10.1016/s0098-3004(99)00141-7), 2000.
- Mudelsee, M.: Break function regression: A tool for quantifying trend changes in climate time series, *Eur. Phys. J.-Spec. Top.*,
480 174(1), 49-63, <https://doi.org/10.1140/epjst/e2009-01089-3>, 2009.
- Nakamura, N., Kayanne, H., Iijima, H., McClanahan, T. R., Behera, S. K., and Yamagata, T.: Footprints of IOD and ENSO in the Kenyan coral record, *Geophys. Res. Lett.*, 38(24), <https://doi.org/10.1029/2011gl049877>, 2011.
- Ólafsdóttir, K. B., and Mudelsee, M.: More accurate, calibrated bootstrap confidence intervals for estimating the correlation between two time series, *Math. Geosci.*, 46(4), 411-427, <https://doi.org/10.1007/s11004-014-9523-4>, 2014.
- 485 Pfeiffer, M., Dullo, W. C., and Eisenhauer, A.: Variability of the Intertropical Convergence Zone recorded in coral isotopic records from the central Indian Ocean (Chagos Archipelago), *Quaternary Res.*, 61(3), 245-255, <https://doi.org/10.1016/j.yqres.2004.02.009>, 2004.
- Pfeiffer, M., and Dullo, W. C.: Monsoon-induced cooling of the western equatorial Indian Ocean as recorded in coral oxygen isotope records from the Seychelles covering the period of 1840–1994 AD, *Quaternary Sci. Rev.*, 25(9-10), 993-1009,
490 <https://doi.org/10.1016/j.quascirev.2005.11.005>, 2006.
- Pfeiffer, M., Timm, O., Dullo, W. C., and Garbe-Schönberg, D.: Paired coral Sr/Ca and $\delta^{18}\text{O}$ records from the Chagos Archipelago: Late twentieth century warming affects rainfall variability in the tropical Indian Ocean, *Geology*, 34(12), 1069-1072, <https://doi.org/10.1130/g23162a.1>, 2006.
- Pfeiffer, M., Dullo, W. C., Zinke, J., and Garbe-Schönberg, D.: Three monthly coral Sr/Ca records from the Chagos
495 Archipelago covering the period of 1950–1995 AD: reproducibility and implications for quantitative reconstructions of sea surface temperature variations, *Int. J. Earth Sci.*, 98(1), 53-66, <https://doi.org/10.1007/s00531-008-0326-z>, 2009.
- Pfeiffer, M., Zinke, J., Dullo, W. C., Garbe-Schönberg, D., Latif, M., and Weber, M. E.: Indian Ocean corals reveal crucial role of World War II bias for twentieth century warming estimates, *Sci. Rep.-UK*, 7(1), 14434, <https://doi.org/10.1038/s41598-017-14352-6>, 2017.
- 500 Quinn, W. H.: The large-scale ENSO event, the El Niño and other important regional features, *Bull. Inst. fr. études andines*, 22(1), 13-34, 1993.
- Reynolds, R. W., Rayner, N. A., Smith, T. M., Stokes, D. C., and Wang, W.: An improved in situ and satellite SST analysis for climate, *J. Climate*, 15(13), 1609-1625, [https://doi.org/10.1175/1520-0442\(2002\)015<1609:aiaisas>2.0.co;2](https://doi.org/10.1175/1520-0442(2002)015<1609:aiaisas>2.0.co;2), 2002.
- Roxy, M., Ritika, K., Terray, P. and Masson, S.: The curious case of Indian Ocean warming, *J. Climate* 27(22), 8501–8509,
505 <https://doi.org/10.1175/JCLI-D-14-00471.1>, 2014.



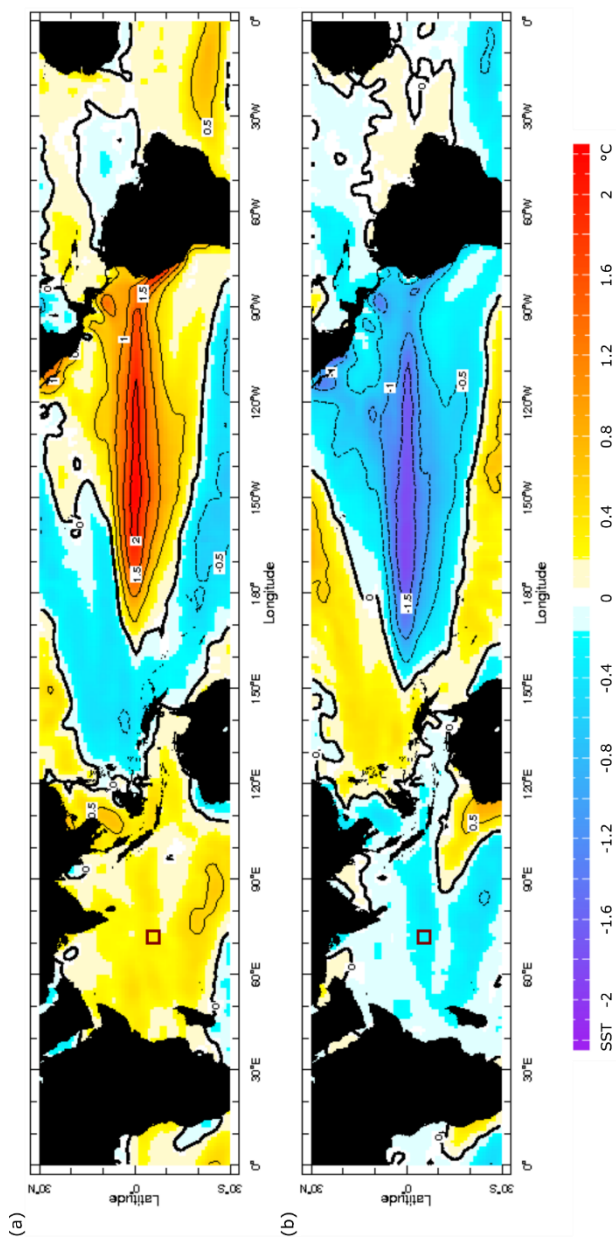
- Sagar, N., Hetzinger, S., Pfeiffer, M., Masood Ahmad, S., Dullo, W. C., and Garbe-Schönberg, D.: High-resolution Sr/Ca ratios in a *Porites lutea* coral from Lakshadweep Archipelago, southeast Arabian Sea: An example from a region experiencing steady rise in the reef temperature, *J. Geophys. Res.-Oceans*, 121(1), 252-266, <https://doi.org/10.1002/2015jc010821>, 2016.
- 510 Saji, N. H., Goswami, B. N., Vinayachandran, P. N., and Yamagata, T.: A dipole mode in the tropical Indian Ocean, *Nature*, 401(6751), 360, <https://doi.org/10.1038/43854>, 1999.
- Saji, N. H., and Yamagata, T.: Structure of SST and surface wind variability during Indian Ocean dipole mode events: COADS observations, *J. Climate*, 16(16), 2735-2751, [https://doi.org/10.1175/1520-0442\(2003\)016<2735:sosasw>2.0.co;2](https://doi.org/10.1175/1520-0442(2003)016<2735:sosasw>2.0.co;2), 2003.
- Sayani, H. R., Cobb, K. M., DeLong, K., Hitt, N. T., and Druffel, E. R.: Intercolony $\delta^{18}\text{O}$ and Sr/Ca variability among *Porites* spp. corals at Palmyra Atoll: Toward more robust coral-based estimates of climate, *Geochem. Geophys. Geosy.*,
515 <https://doi.org/10.1029/2019gc008420>, 2019.
- Schrag, D. P.: Rapid analysis of high-precision Sr/Ca ratios in corals and other marine carbonates, *Paleoceanography*, 14(2), 97-102, <https://doi.org/10.1029/1998pa900025>, 1999.
- Shen, C. C., Cheng, H., Edwards, R. L., Moran, S. B., Edmonds, H. N., Hoff, J. A., and Thomas, R. B.: Measurement of attogram quantities of ^{231}Pa in dissolved and particulate fractions of seawater by isotope dilution thermal ionization mass
520 spectroscopy, *Anal. Chem.*, 75(5), 1075-1079, <https://doi.org/10.1021/ac026247r>, 2003.
- Shen, C. C., Wu, C. C., Cheng, H., Edwards, R. L., Hsieh, Y. T., Gallet, S., ... and Hori, M.: High-precision and high-resolution carbonate ^{230}Th dating by MC-ICP-MS with SEM protocols, *Geochim. Cosmochim. Acta*, 99, 71-86, <https://doi.org/10.1016/j.gca.2012.09.018>, 2012.
- Sheppard, C. R. C., Seaward, M. R. D., Klaus, R., and Topp, J. M. W.: The Chagos Archipelago: an introduction, in: *Ecology of the Chagos Archipelago*, edited by: Shepard, C. R. C., and Seaward, M. R. D., Westbury Academic & Scientific Publishing,
525 Otley, UK, 1-20, 1999.
- Sheppard, C. R. C., Ateweberhan, M., Bowen, B. W., Carr, P., Chen, C. A., Clubbe, C., ... and Gaither, M. R.: Reefs and islands of the Chagos Archipelago, Indian Ocean: why it is the world's largest no-take marine protected area, *Aquat. Conserv.*, 22(2), 232-261, <https://doi.org/10.1002/aqc.1248>, 2012.
- 530 Sheppard, C. R. C., Bowen, B. W., Chen, A. C., Craig, M. T., Eble, J., Fitzsimmons, N., ... and Koldewey, H.: British Indian Ocean Territory (the Chagos Archipelago): setting, connections and the marine protected area, in: *Coral Reefs of the United Kingdom Overseas Territories*, Springer, Dordrecht, NL, 223-240, 2013.
- Smodej, J., Reuning, L., Wollenberg, U., Zinke, J., Pfeiffer, M., and Kukla, P. A.: Two-dimensional X-ray diffraction as a tool for the rapid, nondestructive detection of low calcite quantities in aragonitic corals, *Geochem. Geophys. Geosy.*, 16(10), 3778-
535 3788, <https://doi.org/10.1002/2015gc006009>, 2015.
- Timm, O., Pfeiffer, M., and Dullo, W. C.: Nonstationary ENSO-precipitation teleconnection over the equatorial Indian Ocean documented in a coral from the Chagos Archipelago, *Geophys. Res. Lett.*, 32(2), <https://doi.org/10.1029/2004gl021738>, 2005.
- Vautard, R., and Ghil, M.: Singular spectrum analysis in nonlinear dynamics, with applications to paleoclimatic time series, *Physica D*, 35, 395-424, [https://doi.org/10.1016/0167-2789\(89\)90077-8](https://doi.org/10.1016/0167-2789(89)90077-8), 1989.



- 540 Vialard, J., Duvel, J. P., Mcphaden, M. J., Bouruet-Aubertot, P., Ward, B., Key, E., et al.: Cirene: air–sea interactions in the Seychelles–Chagos thermocline ridge region, *B. Am. Meteorol. Soc.*, 90(1), 45–61, <https://doi.org/10.1175/2008bams2499.1>, 2009.
- Watanabe, T. K., Watanabe, T., Yamazaki, A., Pfeiffer, M., and Claereboudt, M. R.: Oman coral $\delta^{18}\text{O}$ seawater record suggests that Western Indian Ocean upwelling uncouples from the Indian Ocean Dipole during the global-warming hiatus, *Sci. Rep.-UK*, 9(1), 1887, <https://doi.org/10.1038/s41598-018-38429-y>, 2019.
- 545 Webster, P. J., Magana, V. O., Palmer, T. N., Shukla, J., Tomas, R. A., Yanai, M. U., and Yasunari, T.: Monsoons: Processes, predictability, and the prospects for prediction, *J. Geophys. Res.-Oceans*, 103(C7), 14451–14510, <https://doi.org/10.1029/97jc02719>, 1998.
- Webster, P. J., Moore, A. M., Loschnigg, J. P., and Leben, R. R.: Coupled ocean–atmosphere dynamics in the Indian Ocean during 1997–98, *Nature*, 401(6751), 356, <https://doi.org/10.1038/43848>, 1999.
- 550 Wieners, C. E., Dijkstra, H. A., and de Ruijter, W. P.: The Influence of the Indian Ocean on ENSO Stability and Flavor, *J. Climate*, 30(7), 2601–2620, <https://doi.org/10.1175/jcli-d-16-0516.1>, 2017.
- Wilson, R., Cook, E., D'Arrigo, R., Riedwyl, N., Evans, M. N., Tudhope, A., and Allan, R.: Reconstructing ENSO: the influence of method, proxy data, climate forcing and teleconnections, *J. Quaternary Sci.*, 25(1), 62–78, <https://doi.org/10.1002/jqs.1297>, 2010.
- 555 Wu, R., Chen, J., and Chen, W.: Different types of ENSO influences on the Indian summer monsoon variability, *J. Climate*, 25(3), 903–920, <https://doi.org/10.1175/jcli-d-11-00039.1>, 2012.
- Zhang, C.: Madden-Julian Oscillation, *Rev. Geophys.*, 43(2), <https://doi.org/10.1029/2004rg000158>, 2005.
- Zinke, J., Dullo, W.-C., Heiss, G.A., and Eisenhauer, A.: ENSO and Indian Ocean subtropical dipole variability is recorded in a coral record off southwest Madagascar for the period 1659 to 1995, *Earth Planet. Sc. Lett.*, 228(1–2), 177–194, doi: 10.1016/j.epsl.2004.09.028, <https://doi.org/10.1016/j.epsl.2004.09.028>, 2004.
- 560 Zinke, J., Pfeiffer, M., Timm, O., Dullo, W.-C., Kroon, D., and Thomassin, B. A.: Mayotte coral reveals hydrological changes in the western Indian Ocean between 1881 and 1994, *Geophys. Res. Lett.*, 35(23), <https://doi.org/10.1029/2008gl035634>, 2008.
- Zinke, J., Rountrey, A., Feng, M., Xie, S. P., Dissard, D., Rankenburg, K., Lough, J., and McCulloch, M. T.: Corals record long-term Leeuwin Current variability including Ningaloo Niño/Niña since 1795, *Nat. Commun.*, 5, 3607, <https://doi.org/10.1038/ncomms4607>, 2014.
- 565 Zinke, J., Hoell, A., Lough, J. M., Feng, M., Kuret, A. J., Clarke, H., Ricca, V., Rankenburg, K., and McCulloch, M. T.: Coral record of southeastern Indian Ocean marine heatwaves with intensified Western Pacific temperature gradient, *Nat. Commun.*, 6, 8562. <https://doi.org/10.1038/ncomms9562>, 2015.
- 570 Zubair, L., and Ropelewski, C. F.: The strengthening relationship between ENSO and northeast monsoon rainfall over Sri Lanka and southern India, *J. Climate*, 19(8), 1567–1575, <https://doi.org/10.1175/jcli3670.1>, 2006.



595 **Figure 1:** Location of study area and coral sample locations. The Chagos Archipelago is located in the central Indian Ocean, about 550 km south of the Maldives (map upper left). Fossil coral samples were collected on Eagle Island and on Boddam Island (Salomon atoll; red stars).



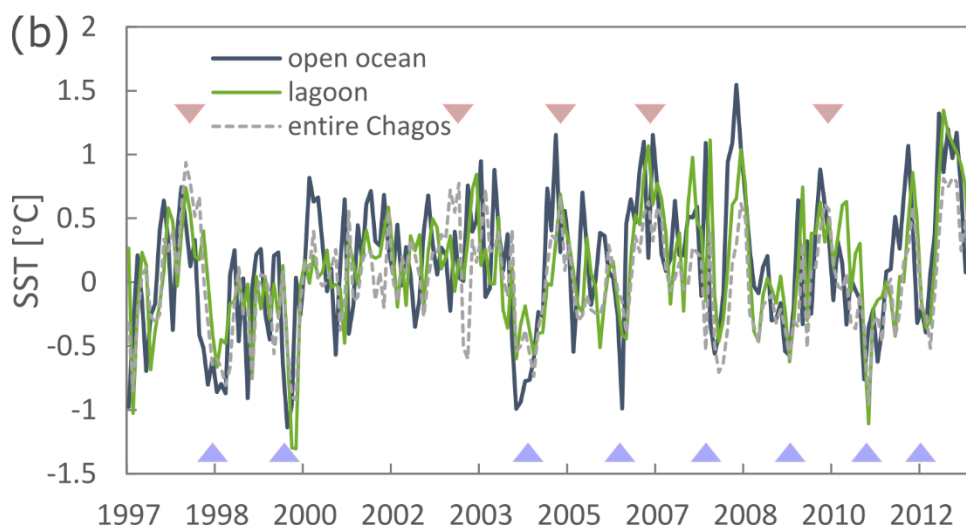
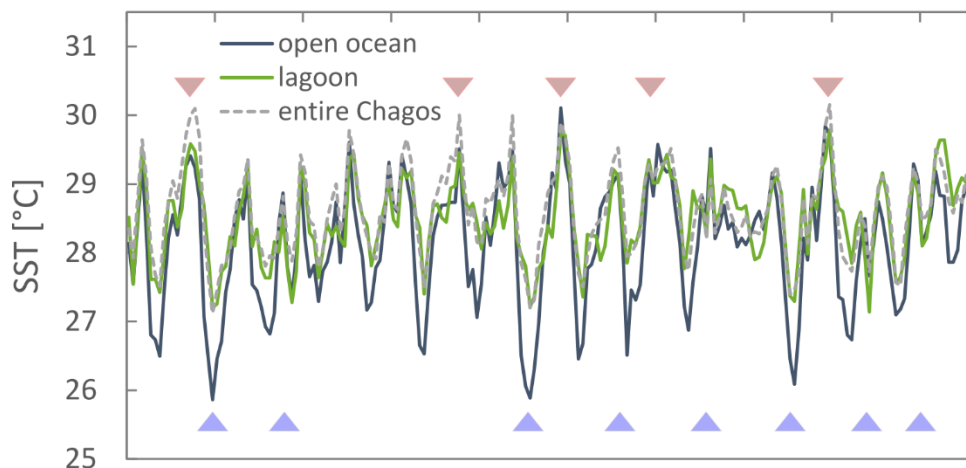
600

Figure 2: Composite maps of SST anomalies [°C] in the Indian and Pacific Ocean during ENSO events. (a) El Niño SST anomalies for the period 1982 to 2016 averaged over December to February. (b) same as in (a), but for La Niña events. SST anomaly maps were computed with NOAA 'Reynolds' OI v2 SST (Reynolds et al., 2002) using the free web application Data Views of the IRI Data Library (<https://iridl.ldeo.columbia.edu/>). Date accessed: 17 September 2018. Red squares indicate the location of the study area. An overview of all events used for each composite map can be found in Table S1 in the supplementary material.

605



(a) 1997 1998 2000 2002 2003 2005 2007 2008 2010 2012



610 **Figure 3: Satellite SST for different settings (lagoon: green; open ocean: blue) and entire Chagos (grey; averaged over 70-74° E; 4-8° S). (a) Monthly satellite SST means and (b) satellite SST anomalies. For the open ocean and lagoon setting we used the high-resolution satellite SST product AVHRR (Casey et al., 2010) and for entire Chagos we used NOAA ‘Reynolds’ OI v2 SST (Reynolds et al., 2002). Arrows indicate El Niño (red) and La Niña events (blue) based on Brönnimann et al. (2006) and the Oceanic Niño Index ONI (<https://www.ggweather.com/enso/oni.htm>; Date accessed: 18 October 2018).**



615

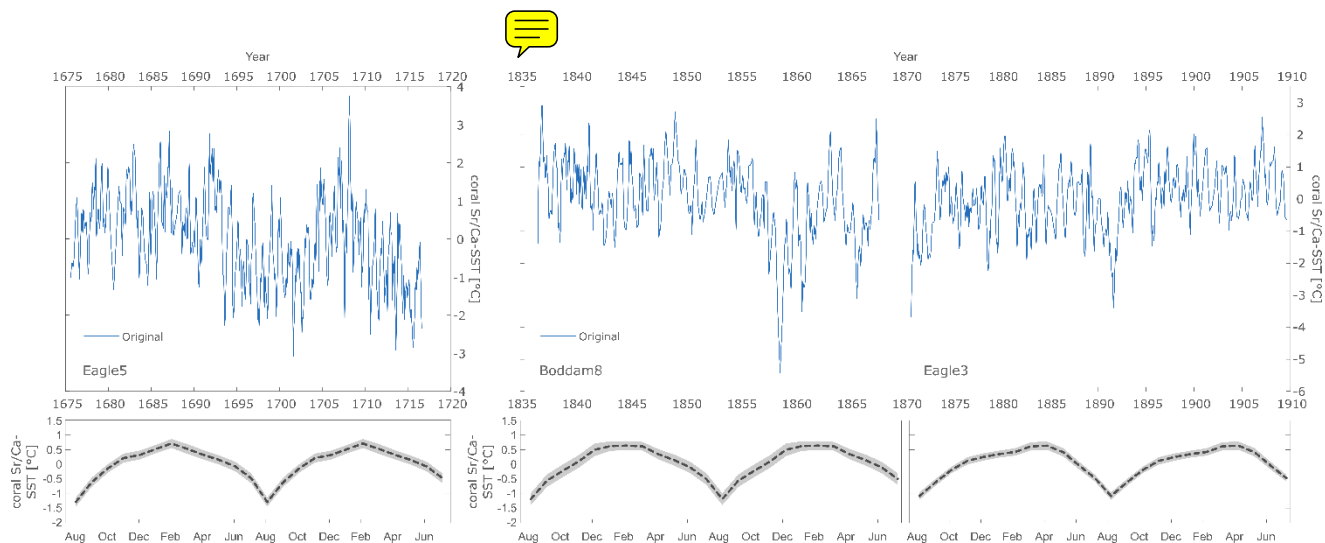
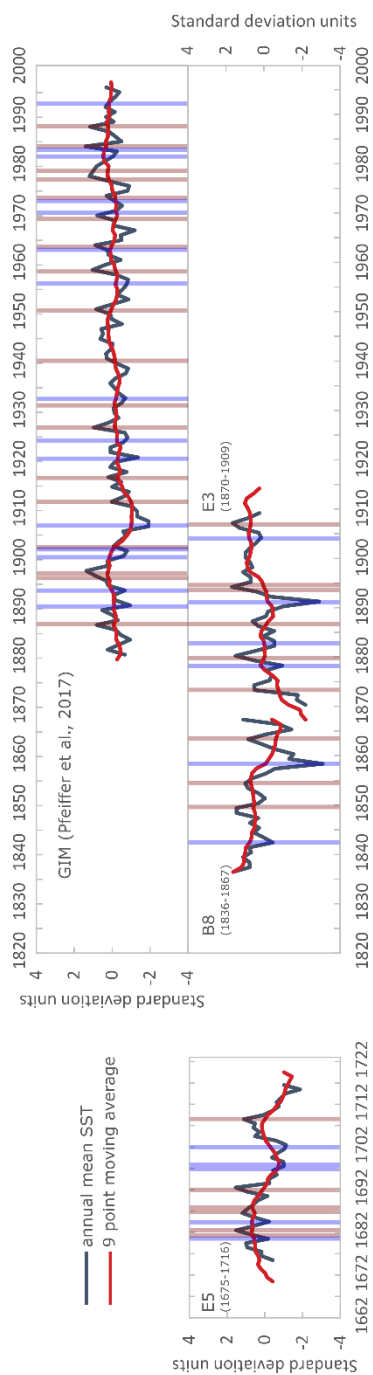
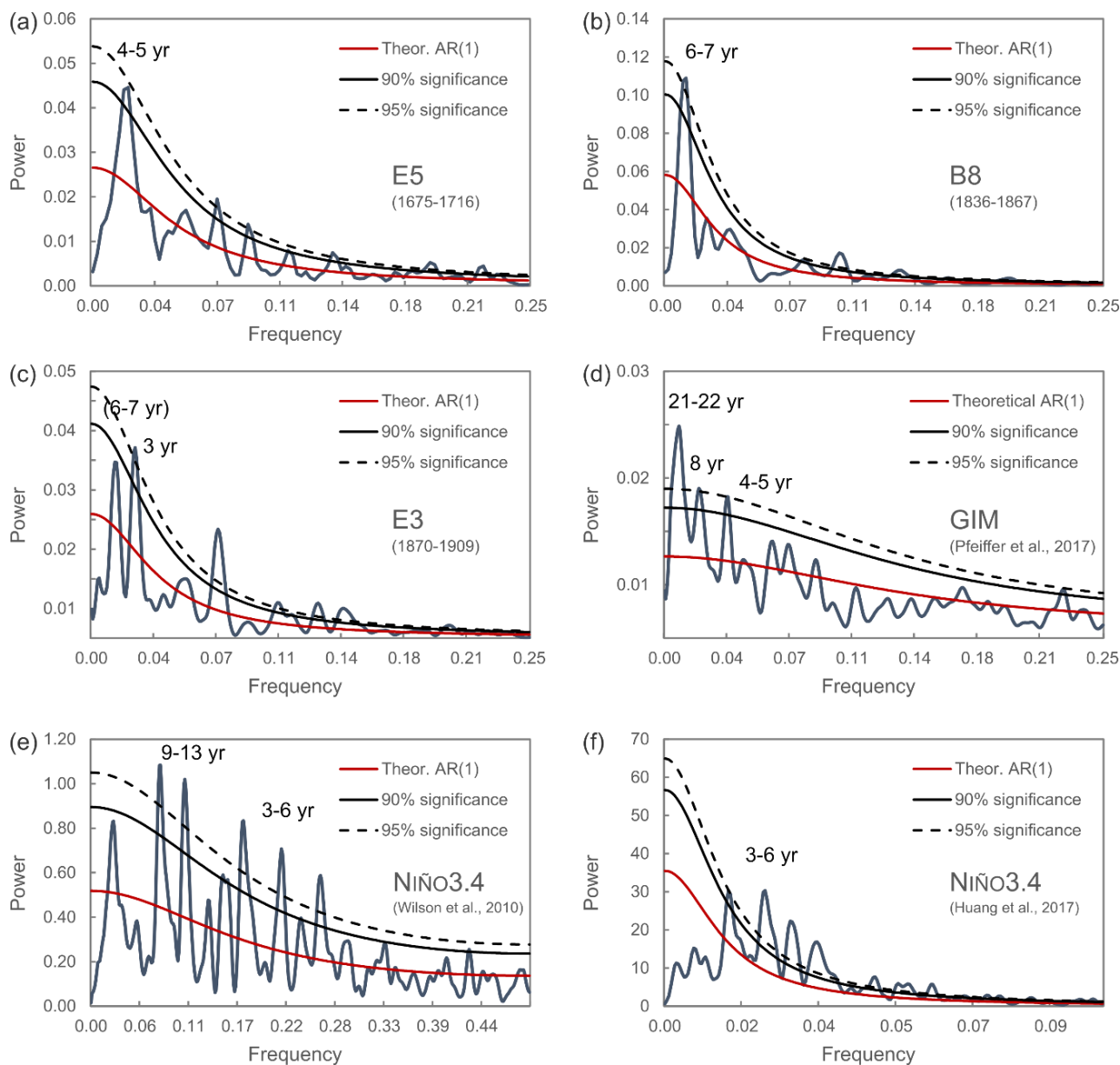


Figure 4: Monthly Sr/Ca records (blue lines; converted into coral Sr/Ca-SST in °C) of E5 (1675-1716), B8 (1836-1867) and E3 (1870-1909) and mean annual cycles (black lines and corresponding standard errors highlighted in gray, lower plot).



620 **Figure 5: Annual SST anomalies for Chagos corals (this study and GIM from Pfeiffer et al. 2009, 2017) Red- (El Niño) and blue- (La Niña) shaded boxes indicate years used for the composite records (Figs. 7-9). Red thick lines are 9 point moving averages. See text Sect. 4.5 for how ENSO events were picked.**

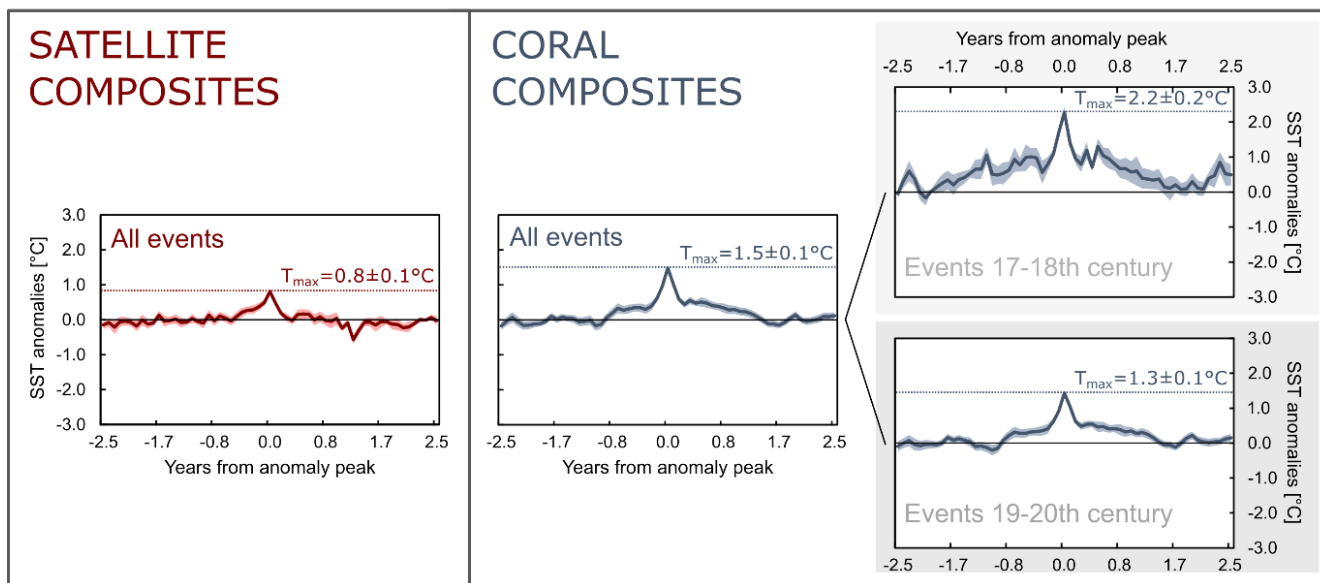


625 **Figure 6: Power spectrum analysis plots for detrended coral SST, the annually resolved Niño3.4 index (Wilson et al., 2010) and the monthly resolved Niño3.4 index based on NOAA ERSSTv5 (Huang et al., 2017) time series.**





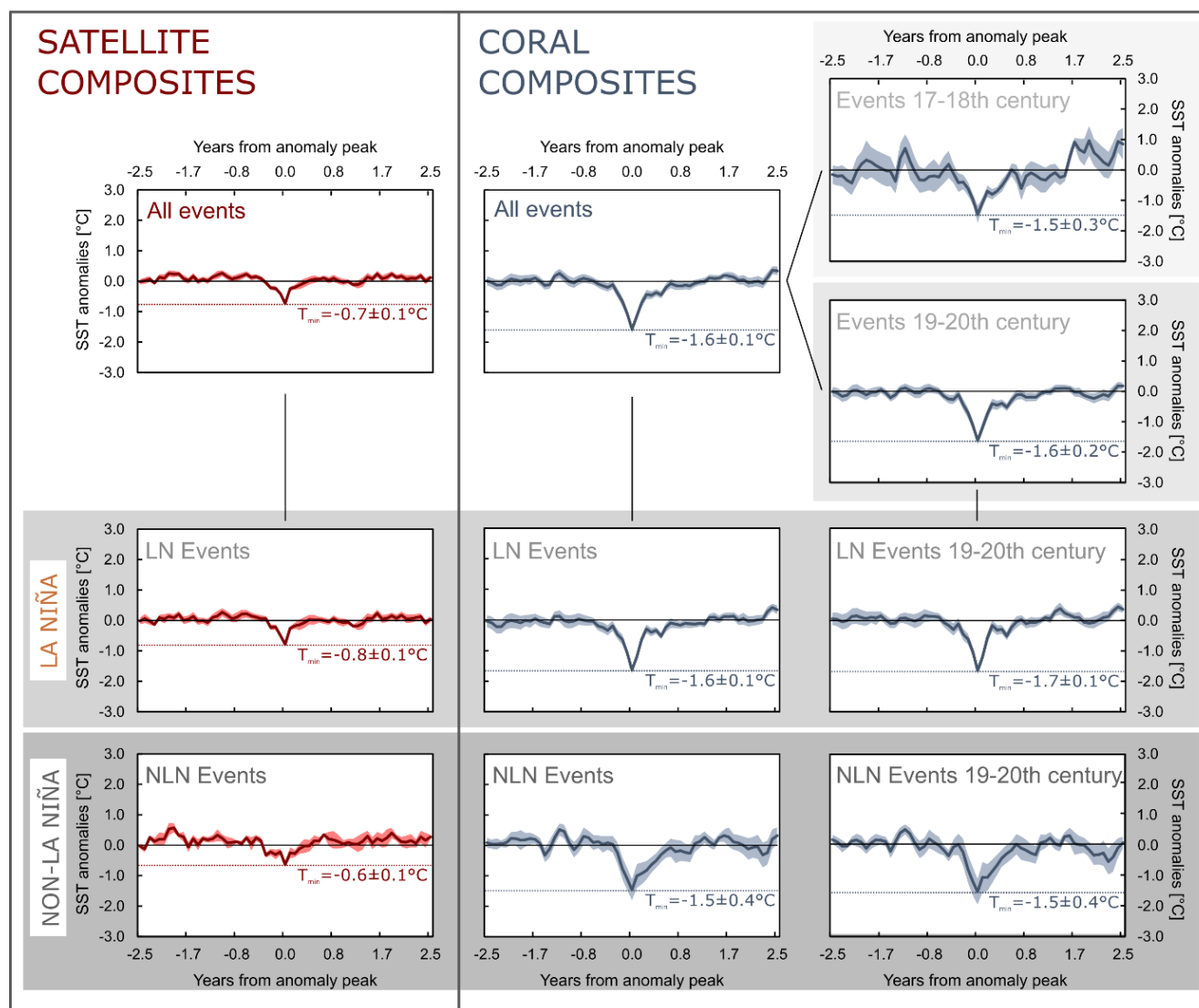
POSITIVE SST ANOMALIES COMPOSITES



630 **Figure 7: Positive SST anomalies (El Niño) composite records of AVHRR (left; red) and coral SST (right; blue) records. Separate composites of anomaly events during the 17-18th and 19-20th century were generated from the coral SST records. Shaded areas below and above the curves show the standard error for the mean values of the composite records. Table 4 for an overview of the events that were selected for generating the composites.**

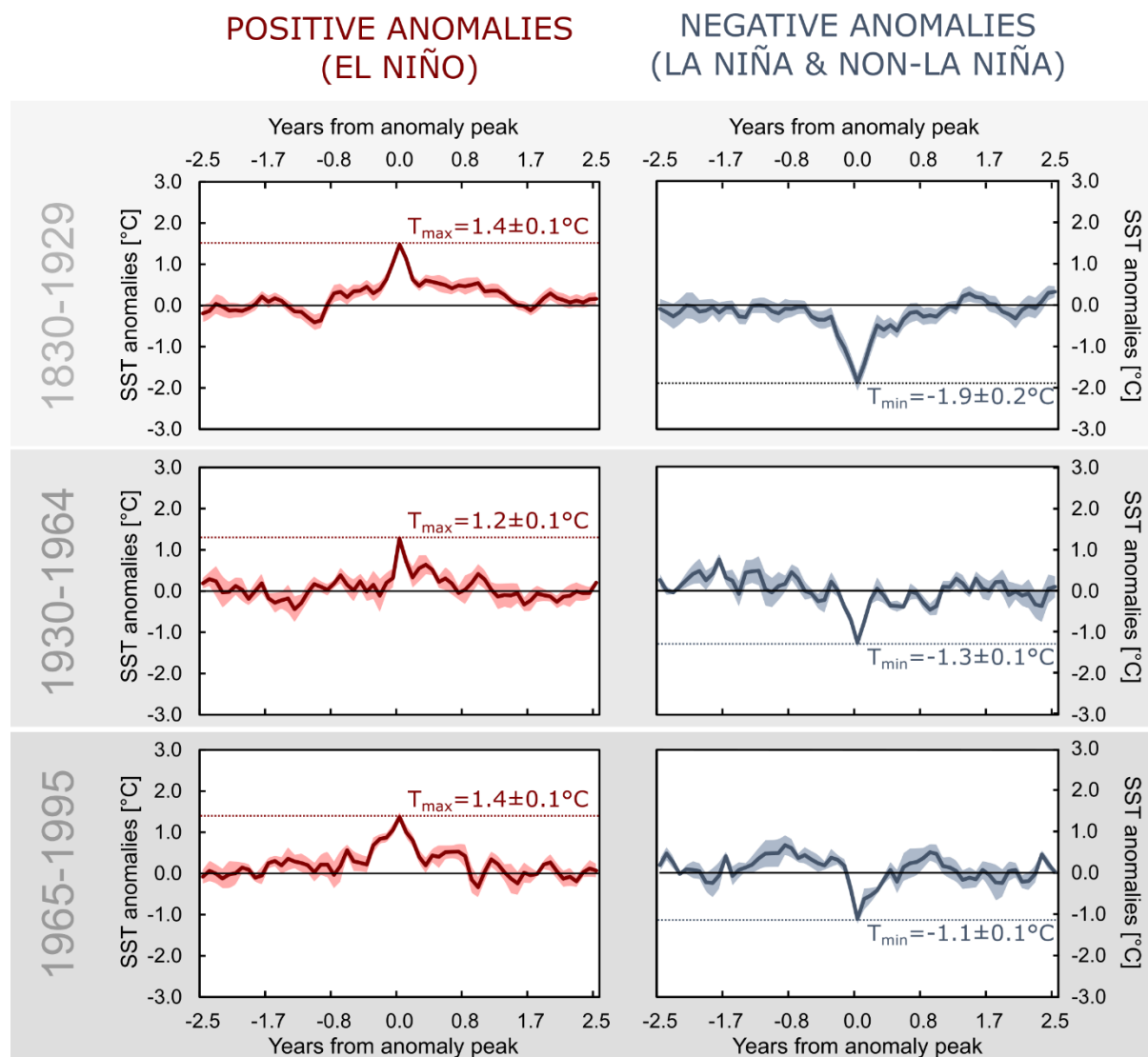


NEGATIVE SST ANOMALIES COMPOSITES



635

Figure 8: Negative SST anomalies (La Niña and non-La Niña) composite records of AVHRR satellite (left) and coral SST (right) records. Additionally, composites of anomaly events separated by 17-18th and 19-20th century events and by La Niña and non-La Niña events were generated. Shaded areas below and above the curves show the standard error for the mean values of the composite records. See Table 4 for an overview of the events that were selected for generating the composites.



640 **Figure 9:** Positive (El Niño; left) and negative SST anomalies (La Niña and non-La Niña; right) composite records of the 19-20th century coral SST records separated by the time intervals 1830-1929 (upper row), 1930-1964 (middle row) and 1965-1995 (lower row). Shaded areas below and above the curves show the standard error for the mean values of the composites records. See Table 5 for an overview of the events that were selected for generating the composites.



645 **Table 1: Overview of Uranium and Thorium isotopic compositions and ^{230}Th ages and corresponding years for fossil coral samples E5 (1675-1716), B8 (1836-1867) and E3 (1870-1909) measured with MC-ICPMS, Thermo Electron Neptune, at NTU. Location of measurement numbers are indicated on x-ray images in Figure S2. Chemistry was performed on March.11th, 2016 and on July 16, 2017 (Shen et al., 2003), and instrumental analysis on MC-ICP-MS (Shen et al., 2012).**

Sample ID	Measurement No.	^{238}U (ppb ^a)	^{232}Th (ppt)	$d^{234}\text{U}$ (measured ^a)	$[\text{}^{230}\text{Th}/\text{}^{238}\text{U}]$ (activity ^c)	$[\text{}^{230}\text{Th}/\text{}^{232}\text{Th}]$ (ppm ^d)	Age (uncorrected)	Age (corrected ^{e,e'})	$d^{234}\text{U}_{\text{initial}}$ (corrected ^b)	Corresponding year (BP)
E5 (1675-1716)	1st	2265,7 ± 2,3	74,1 ± 3,0	146,4 ± 1,3	0,003250 ± 0,000019	1639 ± 66	309,5 ± 1,9	308,8 ± 1,9	146,6 ± 1,3	1706 ± 1,9
	2nd	2293,9 ± 2,2	16,1 ± 1,3	145,0 ± 1,6	0,003594 ± 0,000018	8458 ± 675	342,8 ± 1,8	342,6 ± 1,8	145,2 ± 1,6	1674 ± 1,8
B8 (1836-1867)	1st	2212,7 ± 2,5	37,1 ± 4,1	144,1 ± 1,5	0,001872 ± 0,000023	1840 ± 203	178,5 ± 2,2	178,1 ± 2,2	144,2 ± 1,5	1838 ± 2,2
	2nd	2386,1 ± 2,1	515,4 ± 1,4	146,2 ± 1,3	0,001650 ± 0,000029	126 ± 2	157,1 ± 2,8	152,1 ± 3,7	146,2 ± 1,3	1865 ± 3,7
E3 (1870-1909)	1st	2551,9 ± 2,5	56,7 ± 3,9	145,4 ± 1,3	0,001194 ± 0,000025	886 ± 64	113,8 ± 2,4	113,3 ± 2,4	145,4 ± 1,3	1903 ± 2,4
	2nd	2694 ± 2,8	643 ± 2	144,7 ± 1,7	0,0015 ± 0,00002	106 ± 1	146 ± 2	141 ± 3,2	145 ± 1,7	1876 ± 3,2

Analytical errors are 2σ of the mean.

^a $[\text{}^{238}\text{U}] = [\text{}^{235}\text{U}] \times 137.818 (\pm 0.65\%)$ (Hiess et al., 2012); $\delta^{234}\text{U} = ([\text{}^{234}\text{U}/\text{}^{238}\text{U}]_{\text{activity}} - 1) \times 1000$.

^b $\delta^{234}\text{U}_{\text{initial}}$ corrected was calculated based on ^{230}Th age (T), i.e., $\delta^{234}\text{U}_{\text{initial}} = \delta^{234}\text{U}_{\text{measured}} \times e^{\lambda_{234}T}$, and T is corrected age.

^c $[\text{}^{230}\text{Th}/\text{}^{238}\text{U}]_{\text{activity}} = 1 - e^{-\lambda_{230}T} + (\delta^{234}\text{U}_{\text{measured}}/1000)[\lambda_{230}/(\lambda_{230} - \lambda_{234})](\lambda - e^{-(\lambda_{230} - \lambda_{234})T})$, where T is the age.

655 ^dThe degree of detrital ^{230}Th contamination is indicated by the $[\text{}^{230}\text{Th}/\text{}^{232}\text{Th}]$ atomic ratio instead of the activity ratio.

^eAge corrections, relative to chemistry date, for samples were calculated using an estimated atomic $^{230}\text{Th}/\text{}^{232}\text{Th}$ ratio of 4 ± 2 ppm.

Those are the values for a material at secular equilibrium, with the crustal $^{232}\text{Th}/\text{}^{238}\text{U}$ value of 3.8. The errors are arbitrarily assumed to be 50%.

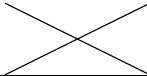
660 **Table 2: Statistical overview for raw Sr/Ca data.**

Sample	Amount subsamples	Sr/Ca [mmol/mol]						median [%]	RSD
		Mean	Median	Std dev	Min	Max	Range		
E5 (1675-1716)	472	8.96	8.96	0.07	8.73	9.14	0.410	0.076	
B8 (1836-1867)	375	9.02	9.02	0.07	8.85	9.36	0.506	0.075	
E3 (1870-1909)	415	8.95	8.95	0.06	8.79	9.17	0.376	0.074	

Table 3: Statistical overview for mean annual cycle data of the coral Sr/Ca-SST [°C] records.

Sample	Max	Min	Amplitude	Mean	SD	P-value of t-test (two-tailed)		
						E5 (1675-1716) vs.	B8 (1836-1867) vs.	E3 (1870-1909) vs.
E5 (1675-1716)	0.70	-1.29	1.99	0.0026	0.5459	0.9979	0.9979	0.9991
B8 (1836-1867)	0.61	-1.21	1.82	0.0033	0.5450	0.9979	0.9979	0.9969



E3 (1870-1909)	0.60	-1.11	1.71	0.0024	0.5089	0.9991	0.9969	
----------------	------	-------	------	--------	--------	--------	--------	---

Note. SD is the standard deviation.



665

Composite		Years with events	Number of events	Records used	
Positive SST anomalies	Coral Composites	all events	1679, 1682, 1686, 1687, 1691, 1708, 1849, 1853, 1863, 1873, 1879, 1881, 1886 (2x), 1889, 1894, 1895, 1896, 1897, 1902, 1907, 1911, 1916, 1926, 1932, 1940, 1951, 1958, 1963, 1969, 1973, 1977, 1979, 1983, 1987	35	E5 (1675-1716), B8 (1836-1867), E3 (1870-1909), GIM (1880-1995)
		17-18th century	1679, 1682, 1686, 1687, 1691, 1708	6	E5 (1675-1716)
		19-20th century	1849, 1853, 1863, 1873, 1879, 1881, 1886 (2x), 1889, 1894, 1895, 1896, 1897, 1902, 1907, 1911, 1916, 1926, 1932, 1940, 1951, 1958, 1963, 1969, 1973, 1977, 1979, 1983, 1987	29	B8 (1836-1867), E3 (1870-1909), GIM (1880-1995)
	Satellite Composite	all events	1983, 1987, 1988, 1998, 2003, 2005, 2007, 2015, 2016	9	AVHRR SST (1981-2018)
Negative SST anomalies	Coral Composites	all events	1680, 1684, 1697, 1698, 1702, 1846, 1858, 1860, 1865, 1872, 1883, 1890, 1891, 1893, 1895, 1900, 1902, 1903, 1906, 1920, 1924, 1932, 1947, 1952, 1956, 1964, 1970, 1974, 1982, 1984, 1994	31 (22 LN, 9 NLN)	E5 (1675-1716), B8 (1836-1867), E3 (1870-1909), GIM (1880-1995)
		17-18th century	1680, 1684, 1697, 1698, 1702	5	E5 (1675-1716)
		19-20th century	1846, 1858, 1860, 1865, 1872, 1883, 1890, 1891, 1893, 1895, 1900, 1902, 1903, 1906, 1920, 1924, 1932, 1947, 1952, 1956, 1964, 1970, 1974, 1982, 1984, 1994	26 (19 LN, 7 NLN)	B8 (1836-1867), E3 (1870-1909), GIM (1880-1995)
	Satellite Composite	all events	1984, 1989, 1989, 1992, 1995, 1996, 1998, 2000, 2004, 2008, 2011, 2012, 2014, 2017	14 (10 LN, 4 NLN)	AVHRR SST (1981-2018)

Table 4: Positive (El Niño) and negative (La Niña and non-La Niña) SST anomaly events picked for generating coral and satellite composite records shown in Figure 7 and Figure 8.



19-20th century Coral Composite	Period	Years with events	Number of events	Records used
Positive SST anomalies	1830-1929	1849, 1853, 1863, 1873, 1879, 1981, 1886 (2x), 1889, 1894, 1895, 1896, 1897, 1902, 1907, 1911, 1916, 1926	18	B8 (1836-1867), E3 (1870-1909), GIM (1880-1995)
	1930-1964	1932, 1940, 1951, 1958, 1963	5	GIM (1880-1995)
	1965-1995	1969, 1973, 1977, 1979, 1983, 1987	6	GIM (1880-1995)
Negative SST anomalies	1830-1929	1846, 1858, 1860, 1865, 1872, 1883, 1890, 1891, 1893, 1895, 1900, 1902, 1903, 1906, 1920, 1924	16	B8 (1836-1867), E3 (1870-1909), GIM (1880-1995)
	1930-1964	1932, 1947, 1952, 1956, 1964	5	GIM (1880-1995)
	1965-1995	1970, 1974, 1982, 1984, 1994	5	GIM (1880-1995)

Table 5: 19-20th century (divided into three periods) positive (El Niño) and negative (La Niña and non-La Niña) SST anomaly events picked for generating coral composite records shown in Figure 9.

670



	Positive SST Anomalies						Negative SST Anomalies			
	Events in Records		Published ENSO events				Events in Records		Published ENSO events	
			Quinn (1993)		Brönnimann et al. (2006)				Brönnimann et al. (2006)	
Years	Numbers of events	Years of very strong (VS), strong (S), medium (M) and weak (W) events	Numbers of events	Years of strong events	Numbers of events	Years	Numbers of events	Years of strong events	Numbers of events	
E5 (1675-1716)	1678/79, 1682/83, 1685/86, 1686/87, 1691/92, 1707/08	6	1681 (S), 1684 (M+), 1687-88 (S+), 1692-93 (S), 1696-97 (M+), 1701 (S+), 1707-09 (M/S), 1715-16 (S)	8	1674, 1675, 1677, 1681, 1682, 1691, 1702	7	1680, 1683/84, 1697, 1697/98, 1702	5	1676, 1678, 1698, 1704	4
B8 (1836-1867)	1848/49, 1853/54, 1862/63	3	1837 (M+), 1844-46 (M/S+), 1850 (M), 1852 (M), 1854 (M), 1857-58 (M), 1860 (M), 1862 (M-), 1864 (S), 1866 (M+), 1867-68 (M+)	11	1833, 1846, 1852, 1856, 1869	5	1845/46, 1858, 1860/61, 1864/65	4	1842, 1847, 1863	3
E3 (1870-1909)	1872/73, 1879/80, 1885/86, 1893/94, 1894/95, 1906/07	6	1871 (S+), 1874 (M), 1877-78 (VS), 1880 (M), 1884 (S+), 1887-89 (M+), 1891 (VS), 1897 (M+), 1899-1900 (S), 1902 (M+), 1904-05 (M-), 1907 (M)	12	1869, 1877, 1878, 1889, 1897, 1900, 1903, 1906, 1912	9	1872, 1882/83, 1891, 1895/96, 1903/04	5	1872, 1887, 1890, 1893, 1904, 1910	6
GIM (1880-1995)*	1880/81, 1885/86, 1888/89, 1896/97, 1897, 1902, 1911/12, 1916/17, 1925/26, 1931/32, 1939/40, 1950/51, 1957/58, 1962/63, 1969/70, 1972/73, 1977/78, 1978/79, 1982/83, 1986/87	20	1880 (M), 1884 (S+), 1887-89 (M-/M+), 1891 (VS), 1897 (M+), 1899-90 (S), 1902 (M+), 1904-05 (M-), 1907 (M), 1910 (M+), 1911-12 (S), 1914-15 (M+), 1917 (S), 1923 (M), 1925-26 (VS), 1930-31 (M), 1932 (S), 1939 (M+), 1940-41 (S), 1943 (M+), 1951 (M-), 1953 (M+), 1957-58 (S), 1965 (M+), 1969 (M-), 1972-73 (S), 1976 (M), 1978-79 (W), 1982-83 (VS), 1987 (M), 1991-92 (M), 1994-95 (M-)	32	1878, 1889, 1897, 1900, 1903, 1906, 1912, 1915, 1919, 1926, 1931, 1940, 1941, 1952, 1958, 1966, 1973, 1977, 1983, 1987, 1992	21	1889/90, 1893, 1899/00, 1901/02, 1906, 1919/20, 1924, 1931/32, 1947, 1956, 1951/52, 1964, 1970, 1973/74, 1982, 1983/84, 1993/94	17	1887, 1890, 1893, 1904, 1910, 1917, 1925, 1934, 1943, 1950, 1956, 1968, 1971, 1974, 1976, 1985, 1989	17
AVHRR*	1982/83, 1986/87, 1987/88, 1997/98, 2002/03, 2004/05, 2006/07, 2014/15, 2015/16	9	1982/83 (VS), 1986/87 (M), 1987/88 (S), 1991/92 (S), 1994/95 (M), 1997/98 (VS), 2002/03 (M), 2004/05 (W), 2006/07 (W), 2009/10 (M), 2014/15 (W), 2015/16 (VS)	12	/ /	/ /	1984/85, 1989, 1989, 1992, 1995, 1996/97, 1998/99, 1999/00, 2004, 2007/08, 2010/11, 2011/12, 2014, 2016/17	14	1983/84 (W), 1984/85 (W), 1988/89 (S), 1992, 1995/96 (M), 1996/97, 1998/99 (S), 1999/00 (S), 2000/01 (W), 2004, 2005/06 (W), 2007/08 (S), 2008/09 (W), 2010/11 (S), 2011/12 (M), 2014, 2016/17 (W), 2017/18 (W)	18

* Note: Recent events (from 1980 on) were additionally picked using events listed on this website: <https://www.ggweather.com/enso/oni.htm> (Date accessed: 18 October 2018)

Table 6: Overview of all events found in the coral Sr/Ca records and of ENSO events of the corresponding time periods listed in publications. Events in coral records were matched with published events in consideration of age model uncertainties of each coral record.

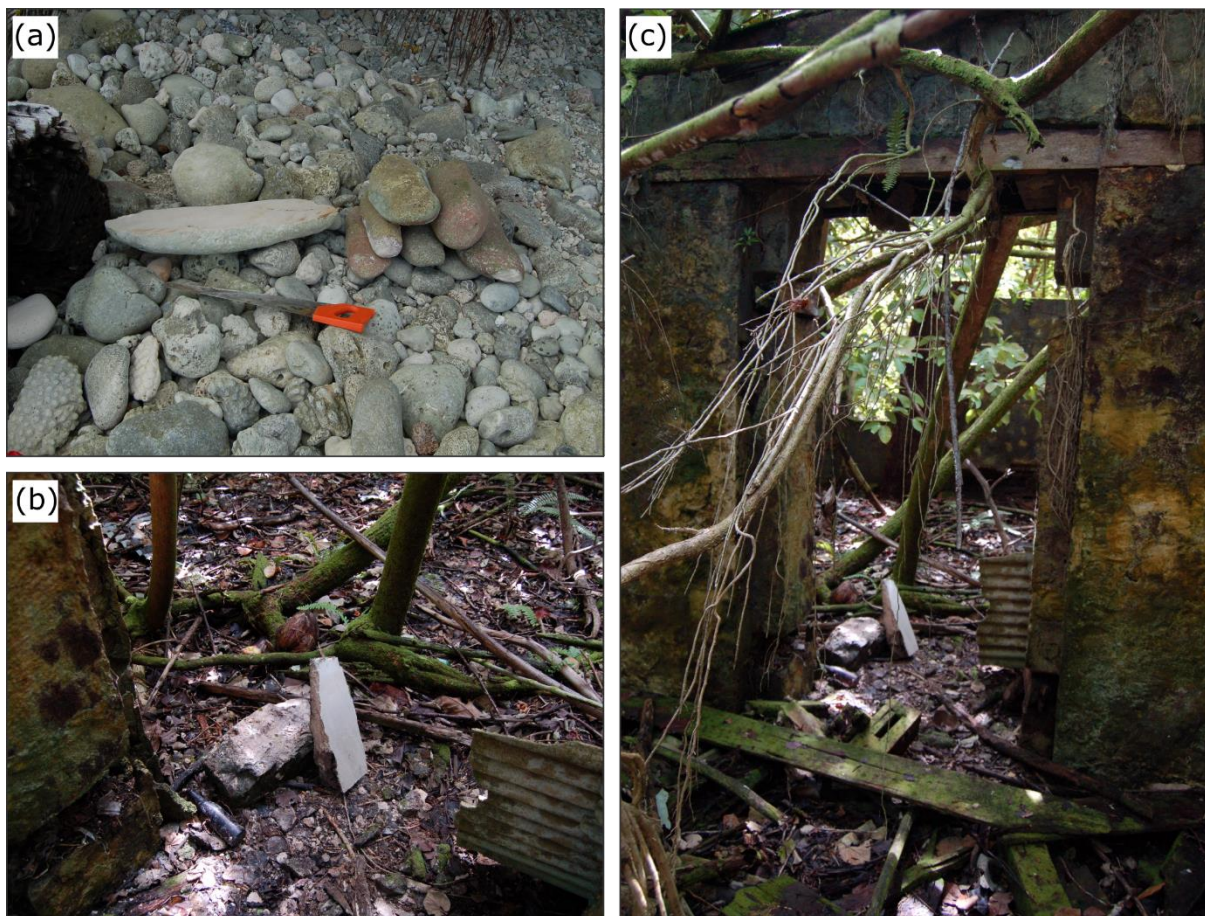
Introduction. This file includes pictures of sampling locations (Fig. S1), x-ray images of the coral samples (Fig. S2), photomicrographs of the coral samples (Figs. S3-S5), plots with Sr/Ca-SST anomalies and anomalies after detrending (Fig. S6), power spectrum analysis plots of non-detrended coral SST anomalies (Fig. S7) and SSA analysis plots (Figs. S8-S10) including text descriptions. Wavelet coherence plots (Fig. S11) and their text description, which support the power spectrum analysis plots in the main manuscript, are included in this file. Two additional tables giving the years of ENSO events used for the composite maps (Table S1) and the linear regression results between the coral SST records and the El Niño index Niño3.4 (Table S2) are also part of this supplementary material.

S1 Table with years of events that were used in the composite maps (Fig. 2)

Event years	
El Nino	La Nina
1982/83	1984/85
1986/87	1988/89
1987/88	1995/95
1991/92	1998/99
1994/95	1999/00
1997/98	2007/08
2002/03	2010/11
2009/10	2011/12
2015/16	

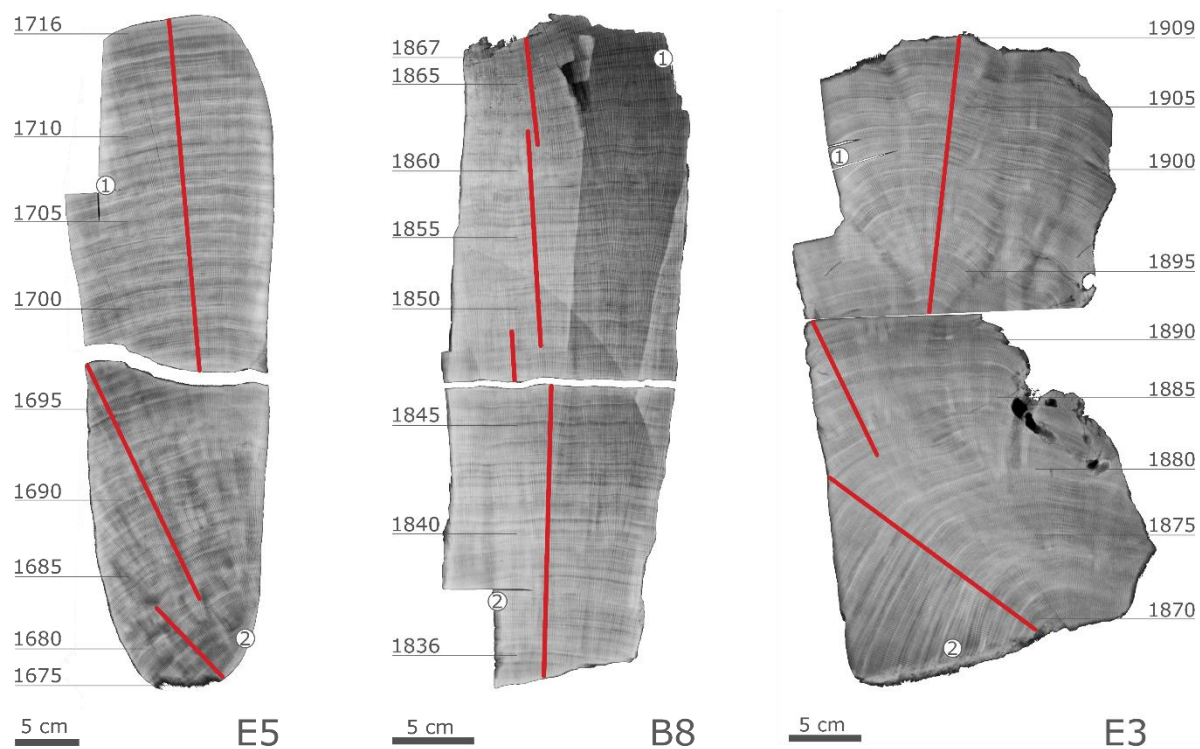
10 **Table S1: El Niño and La Niña events years used for the composite maps. Between 1982 and 2016, 9 El Niño events occurred and 8 La Niña events occurred. Temperature anomalies from December to February were averaged for each event**

S2 Pictures of coral sample sites



- 15 **Figure S1: Pictures of coral sample sites. (a) Boulder beach at Eagle Island where the samples E5 (1675-1716) and E3 (1870-1909) were collected. (b) and (c) a derelict building at Boddam Island from which the sample B8 (1836-1867) was collected.**

S3 X-ray images



20 **Figure S2: X-Ray images of coral samples analyzed in this study. Age models were interpreted using two U/Th measurements from each sample (sampling points for U/Th dating are indicated with circled numbers; for determined ages see Table 1). Red lines indicate subsampling paths.**

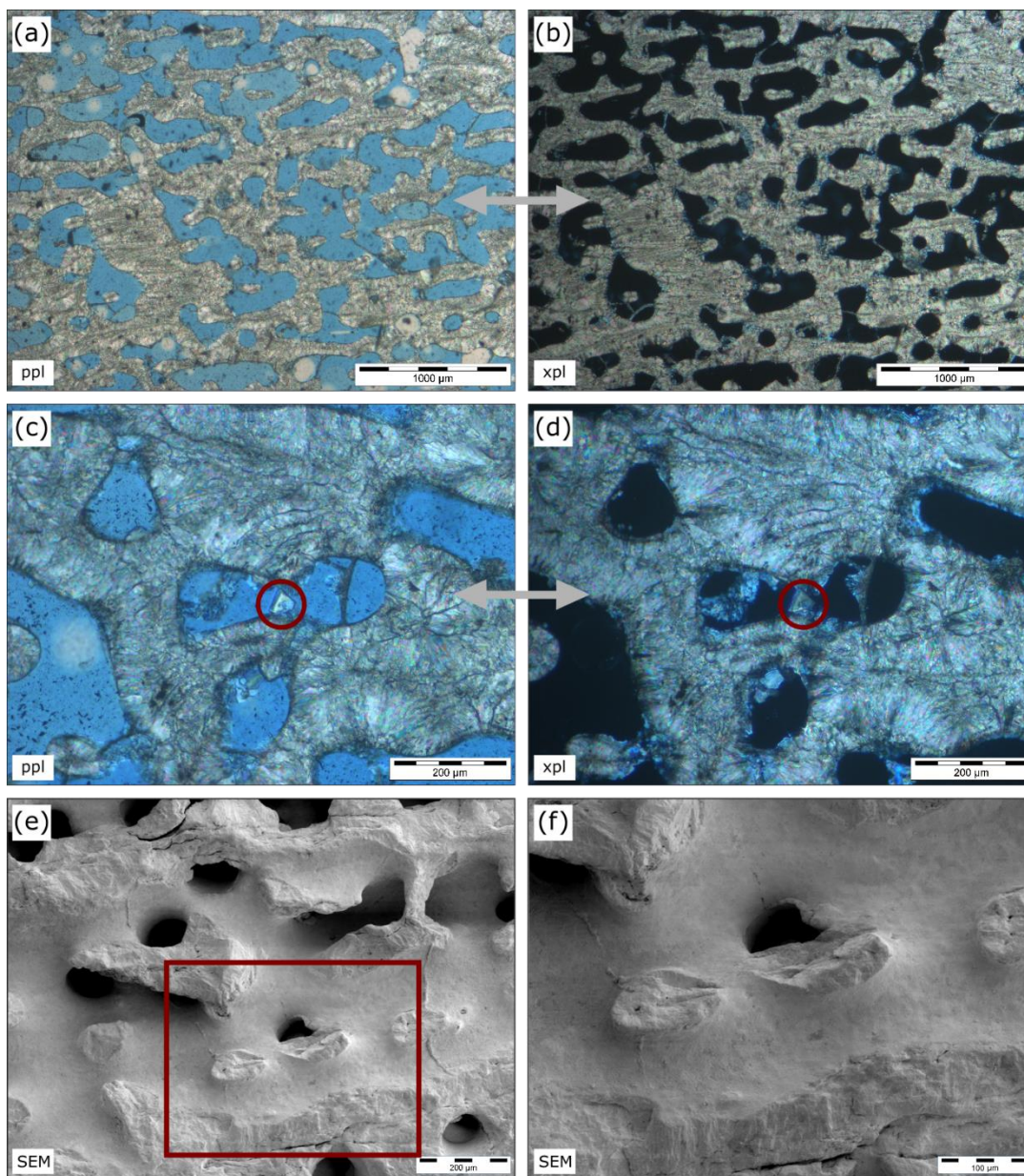


Figure S3: Photomicrographs of coral sample E5 (1675-1716). Double arrows indicate corresponding photomicrographs. (a) PPL and (b) XPL overview photomicrograph of the coral skeleton. (c) PPL and (d) XPL photomicrograph of higher resolution where minor amounts of secondary calcite cement is visible (red circle). (e) SEM overview and (f) SEM detail image of (e) where only trace amounts of sugary cements can be found.

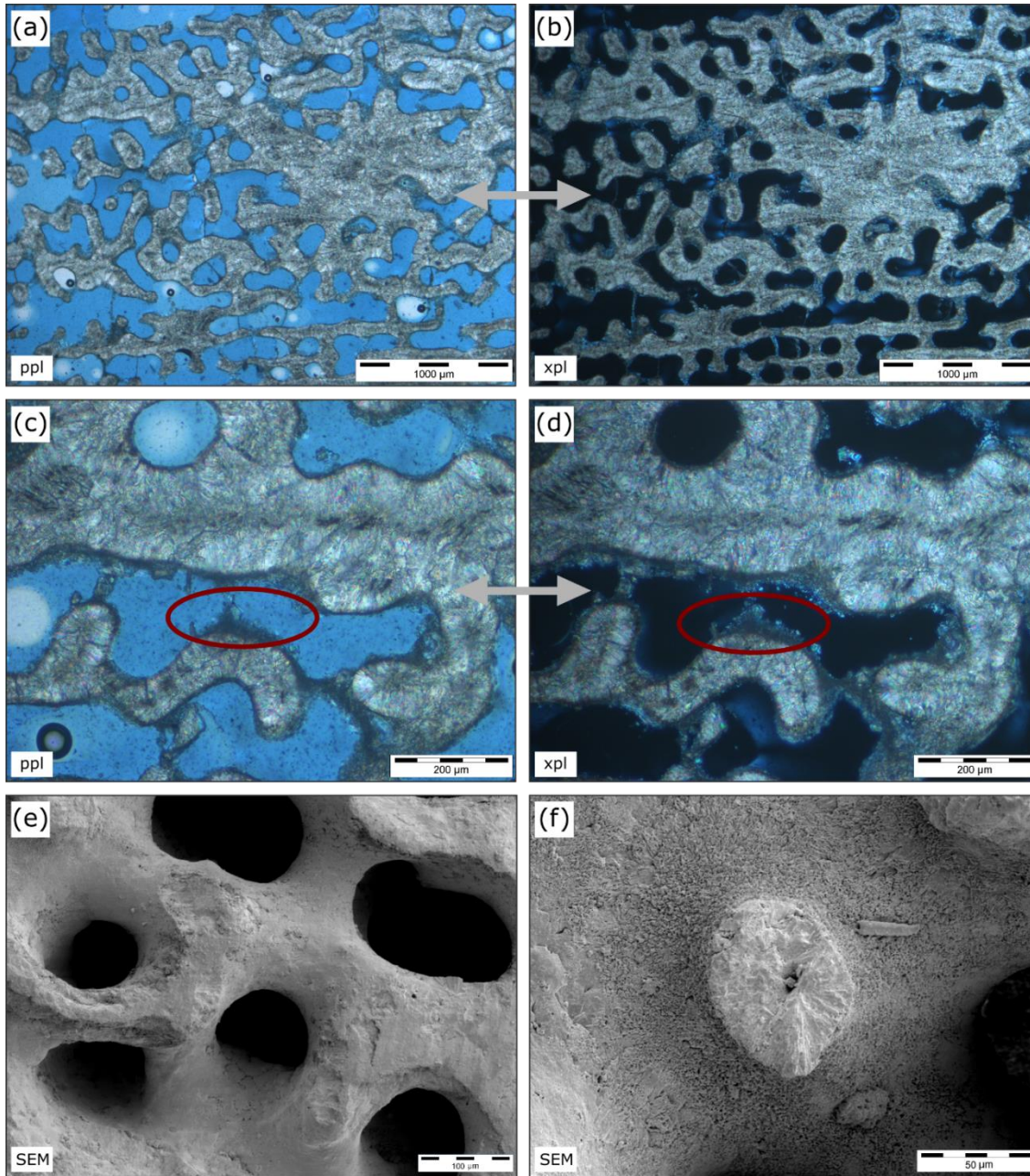


Figure S4; Photomicrographs of coral sample B8 (1836-1867). Double arrows indicate corresponding photomicrographs. (a) PPL and (b) XPL overview photomicrograph of the coral skeleton. (c) PPL and (d) XPL photomicrograph of higher resolution where small amounts of secondary aragonite cement is visible (red oval). (e) SEM overview image and (f) SEM detail image of B8 (1836-1867). Small amounts of sugary aragonitic cement can be seen.

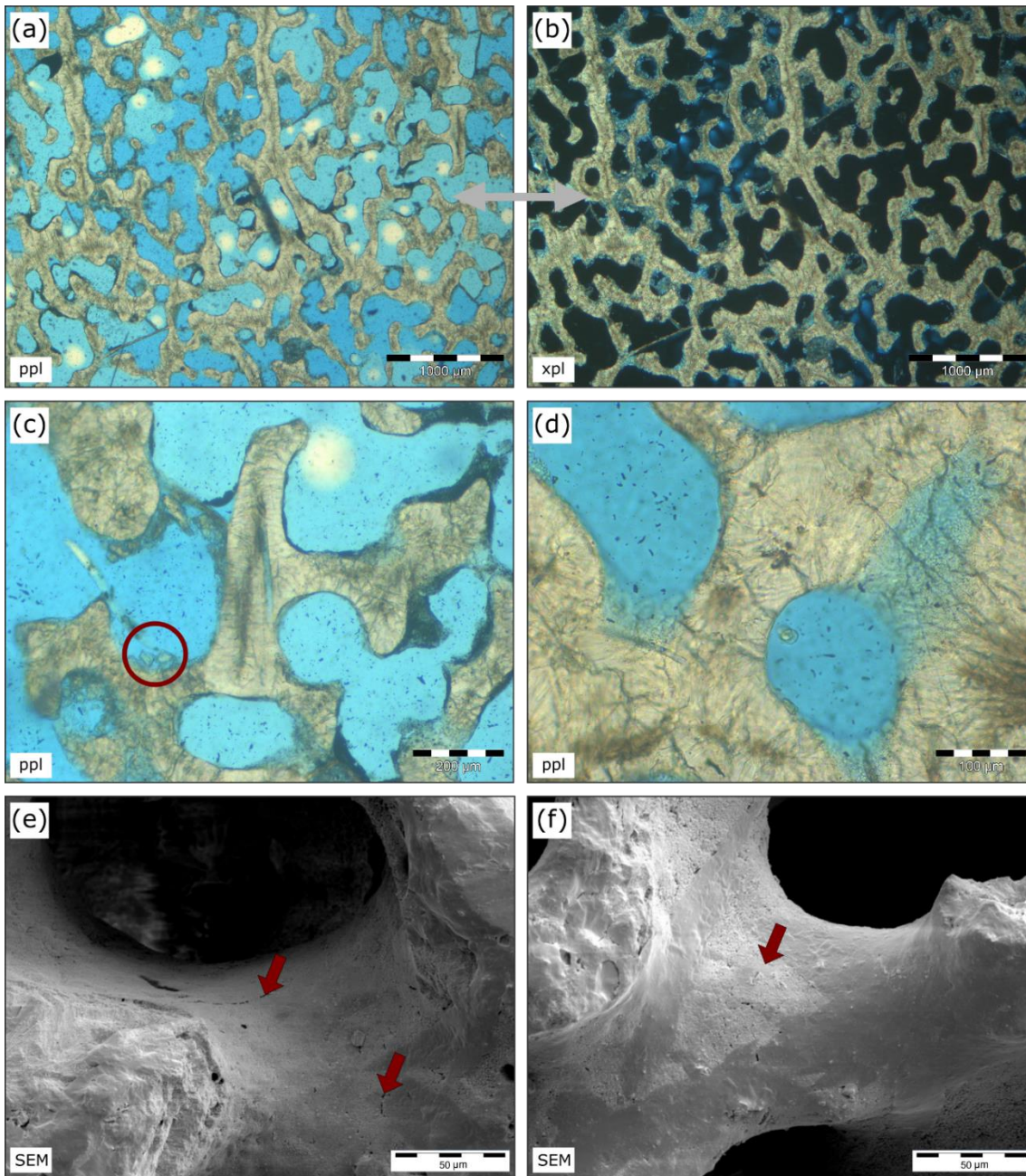
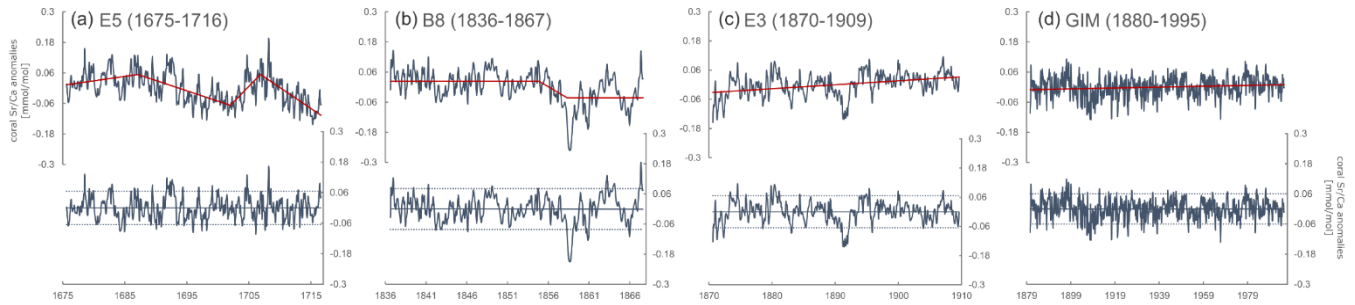


Figure S5: Photomicrographs of coral sample E3 (1870-1909). Double arrows indicate corresponding photomicrographs. (a) PPL and (b) XPL overview photomicrograph of the coral skeleton. (c) PPL photomicrograph of higher resolution where small fragments of aragonite are found (red circle). (d) PPL microphotograph of higher resolution with no signs of diagenesis. SEM images showing (e) microborings (red arrows) and (f) areas which appear brighter due to dissolution.

40

S4 Detrending of coral SST records



45 **Figure S6: Sr/Ca-SST anomalies with calculated trend lines (red lines; upper plot) and anomalies after detrending (lower plot; with plotted 1.5x of the standard deviation as dashed lines) for the coral records (a) E5 (1675-1716), (b) B8 (1836-1867), (c) E3 (1870-1909) and (d) GIM (1880-1995).**

S5 Seasonal cycles inferred from Singular Spectrum Analysis

50 Singular spectrum analysis (SSA) of the coral records with seasonal cycles reveal large interannual to decadal SST variabilities during both the 17-18th century and 19-20th century (not shown). The reconstructed components 2 and 3 (RC2, RC3) produced by SSA describe seasonal amplitudes for all samples and explain 28% (E5), 26% (B8), 32% (E3) of the coral Sr/Ca-SST variance. Decadal variabilities are larger during 17-18th century compared to 19-20th century. The first reconstructed component (RC1) for E5 with seasonal cycles explains 48% of the coral Sr/Ca-SST variance and describes a periodicity of
55 around 18 years. Coral record covering the 19-20th century, lack a reconstructed component produced by SSA that describes decadal variability. Instead, RC1 explains 49% (B8) and 39% (E3) of the coral Sr/Ca-SST variance and describes a periodicity of around 7 years, which can be interpreted as ENSO periodicity.

The SSA results were validated by power spectrum analysis of bimonthly coral SST anomalies, which were not detrended (Fig. S7). To this analysis, the coral record GIM (Pfeiffer et al., 2017) was added. Power spectrum analysis of E5 (Fig. S7a)
60 shows a low-frequency band corresponding to a periodicity of 18-19 years, identical to RC1 of the SSA. In addition, RC2 describing an ENSO periodicity of 4-5 years is confirmed by the second highest low-frequency band in power spectrum analysis of E5. The power spectrum analysis of the corals covering the 19-20th century (B8 and E3) confirms their SSA results, as well (Figs. S7b & c). It shows high power on the low-frequency (5-6 years for B8; 6-7 years for E3) band, which were also described by the first reconstructed components in SSA. Power spectrum analysis for GIM (Fig. S7d) reveals high power on
65 the ENSO band (4-5 years and 8 years) and the highest power on the decadal frequency (26 years).

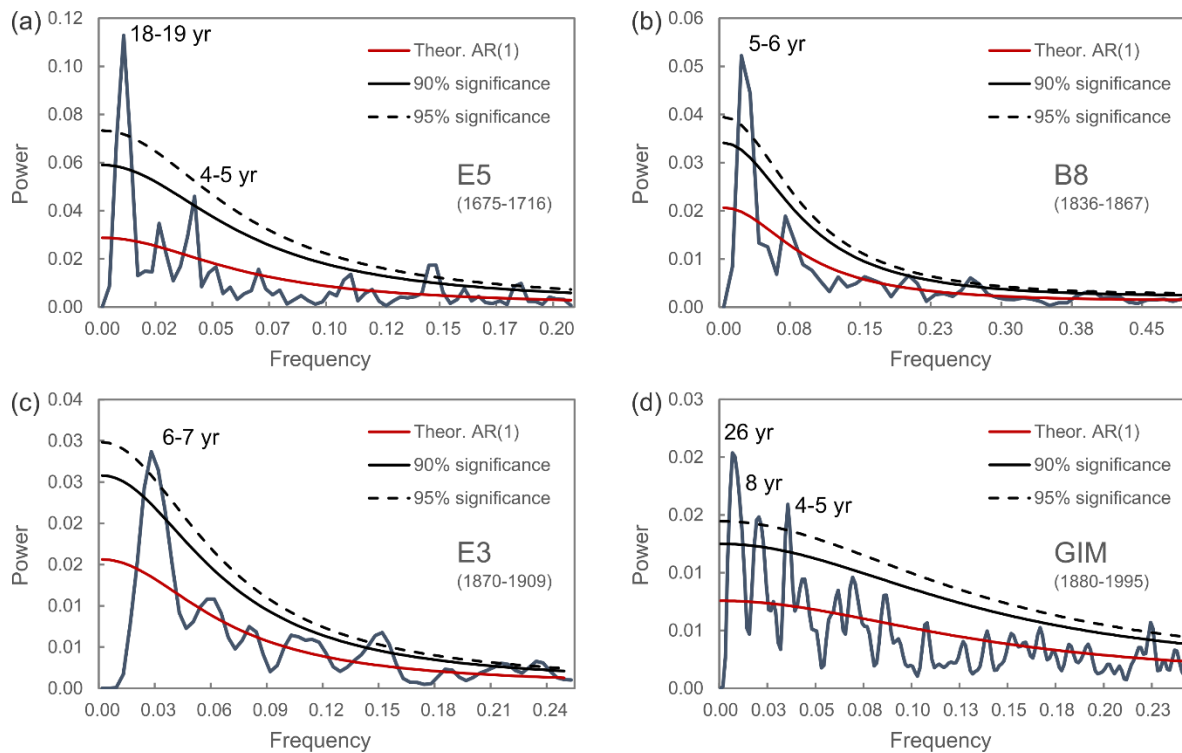


Figure S7: Power spectrum analysis of each Chagos coral bimonthly anomaly series.

70

S6 Interannual SST variability inferred from Singular Spectrum Analysis

The power spectrum analysis results were validated by singular spectrum analysis (SSA) with coral SST anomalies records, to reveal stronger patterns of variance when seasonal cycles were subtracted out (Figs. S8-S10). Still, but of minor percentage (9%), pattern of variance describing the seasonal cycles are found in the third reconstructed component for E5 (1675-1716) and B8 (1836-1867). During the 17-18th century, the coral record shows a periodicity of 18 years in RC1, which explains 47% of the coral Sr/Ca-SST variance (Fig. S8). The second reconstructed component (RC2; Fig. S8) of E5 (1675-1716) explains 14% of the coral Sr/Ca-SST variance and describes an ENSO periodicity of 4-5 years. During the 19-20th century, the pattern of variance describing the ENSO periodicity in the coral records are found in two to three reconstructed components: For B8 (1836-1867), RC2 and RC3 describe an ENSO periodicity of 5-8 years with, in total, 62% of the corals Sr/Ca-SST variability (Fig. S9). For E3 (1870-1909) it is even higher with RC1-3 explaining 65% of the coral Sr/Ca-SST variance. Those three components describe a characteristic ENSO periodicity of 3-8 years (Fig. S10).

80

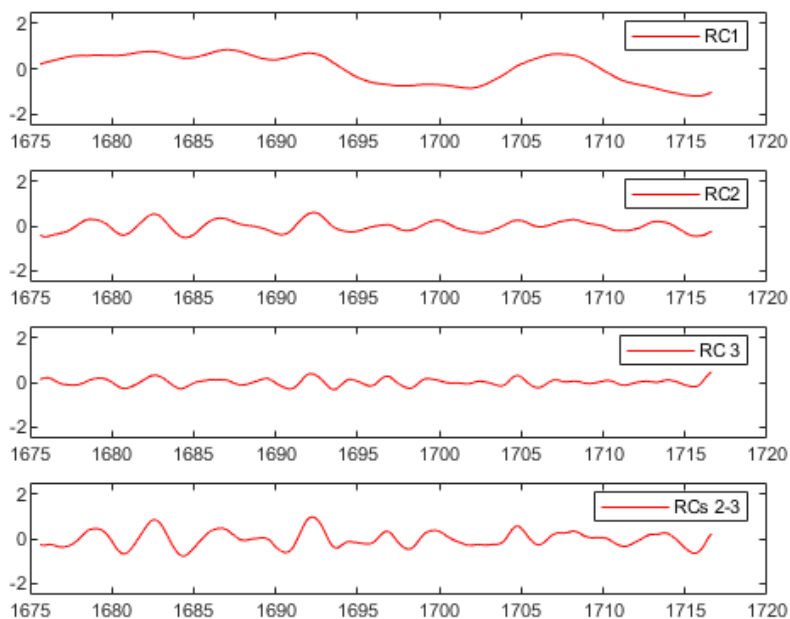


Figure S8: Reconstructed components from Singular Spectrum Analysis of E5 (1675-1716) Sr/Ca monthly anomalies. First reconstructed component (RC1) describes a periodicity of 18 years. RC2 and RC3 describe typical ENSO periodicities.

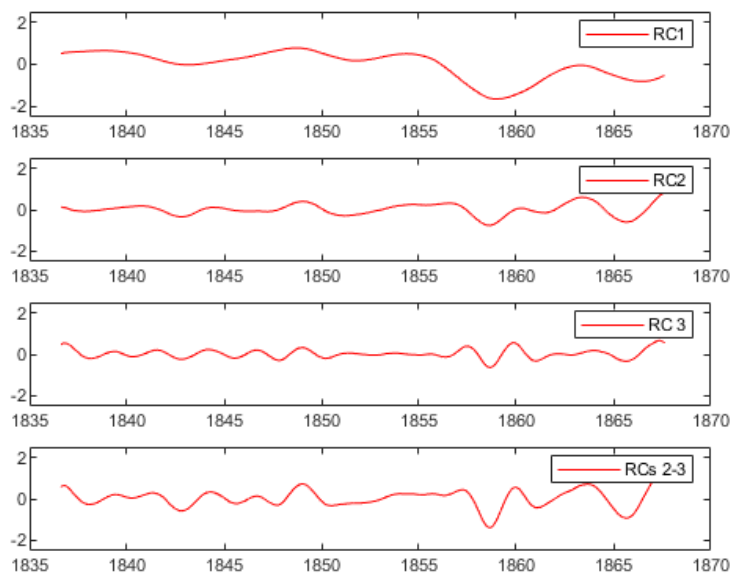


Figure S9: As Figure S8, but for coral Sr/Ca record of B8 (1836-1867).

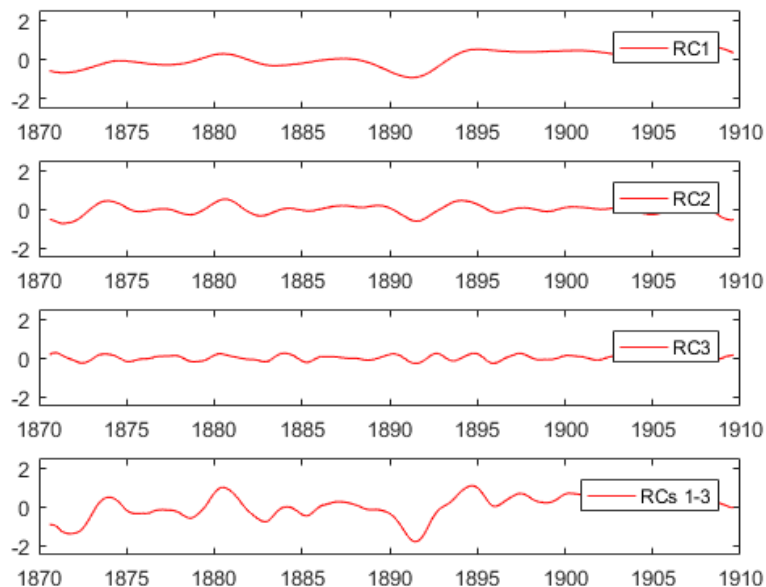


Figure S10: As Figures S8 and S9, but for coral Sr/Ca record of E3 (1870-1909) and ENSO periodicities are described by all shown reconstructed components RC1-3.

90

S7 Wavelet Coherence Analysis

To further investigate the relationship between the coral proxies and ENSO, Wavelet Coherence (WTC) was conducted on all coral records and the Nino3.4 index (Wilson et al., 2010).

Wavelet Coherence (WTC) plots were generated to find regions in time-frequency space where the *Nino3.4* index and the Chagos coral SST records co-vary, even if they do not have high power in those regions (Fig. S11).

All WTC plots of the *Nino3.4* index and coral SST records reveal time-localized areas of strong coherence occurring in periods that correspond to the characteristic ENSO cycles of two to eight years. The WTC plots for the Nino3.4 index and the 19-20th century coral records show several regions where both time series co-vary. In contrast, the WTC plot of the *Niño3.4* index and the 17-18th century coral SST record shows only one region of co-variation at the beginning of the 18th century. The plots show that there is an approximate delay of a 9 months to one year between the 17-18th century coral SST record and the Niño3.4 index (Fig. S11a), an approximate 1-3 year lag between B8 (1836-1867) and E3 (1870-1909), respectively, and the Nino3.4 index (Figs. S11b & c). However, the lags between the coral SST and the index time series are rather a result of the age model uncertainties than real time lags.

105

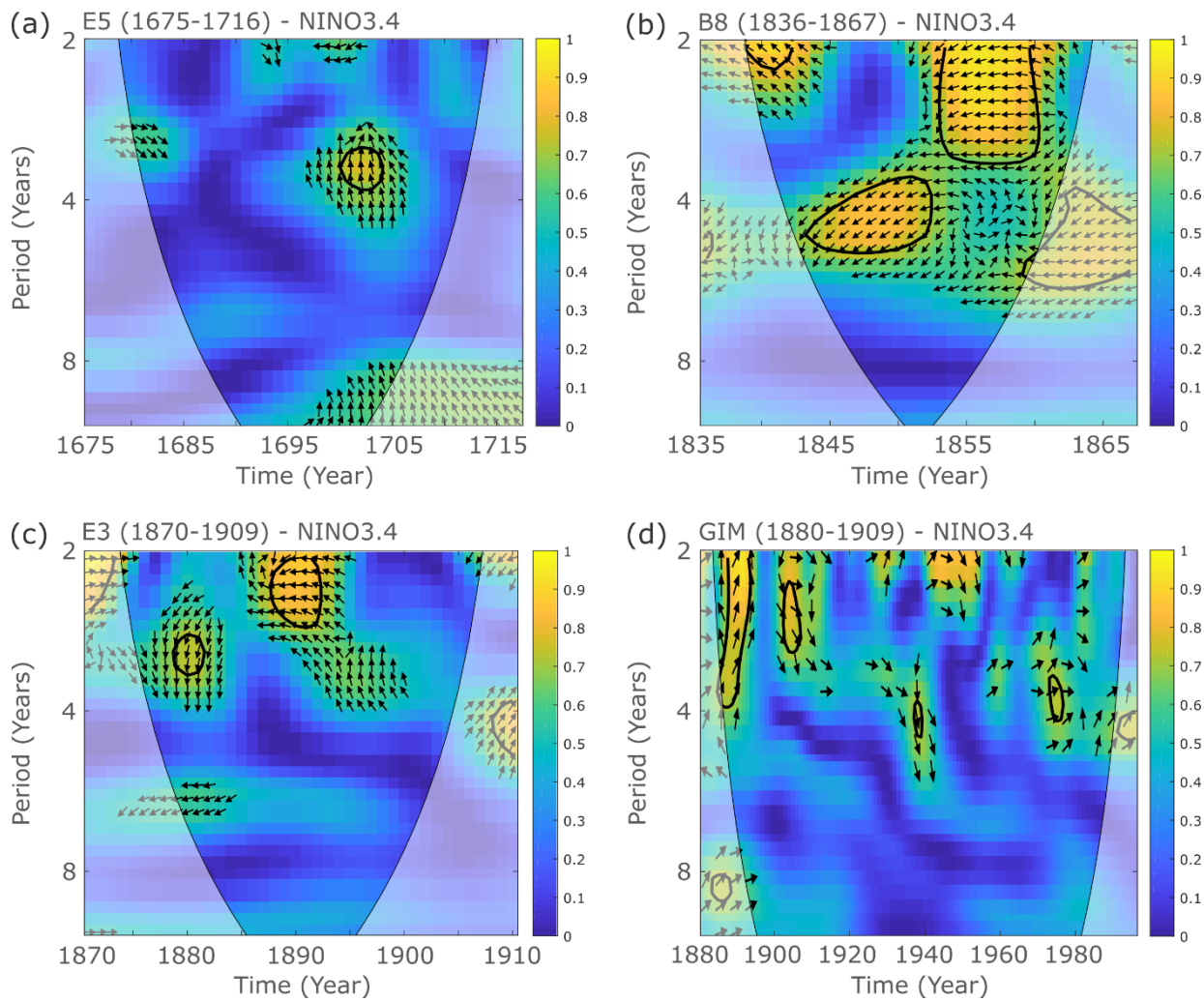


Figure S11: Wavelet coherence analysis plots for the Nino3.4 index and Chagos coral SST of (a) E5 (1675-1716), (b) B8 (1836-1867), (c) E3 (1870-1909) and (d) GIM (1880-1995).



110 **S8 Linear regression**

Ordinary least square (OLS) regression and *PearsonT3* calculation results reveal no significant linear relation between annual coral SST records and the El Niño index *Niño3.4* (Table S2).

Method	Coefficient	E5 (1675-1716)	B8 (1836-1867)	E3 (1870-1909)	GIM (1880-1995)
Excel OLS	R ² (p-value)	4.09E-5 (0.9679)	0.0006 (0.8979)	0.0027 (0.7502)	0.0444 (0.0232)
PearsonT3	r [95% confidence interval]	-0.006 [-0.361; 0.350]	-0.024 [-0.739; 0.716]	0.052 [-0.418; 0.500]	0.211 [-0.005; 0.408]

Table S2: Correlation coefficients of given coral records with the Niño3.4 index.